

MAPSS: MANIFOLD-BASED ASSESSMENT OF PERCEPTUAL SOURCE SEPARATION

Amir Ivry¹ Samuele Cornell² Shinji Watanabe²

¹Electrical and Computer Engineering, Technion – Israel Institute of Technology, Haifa, Israel

²Language Technologies Institute, Carnegie Mellon University, Pittsburgh, PA, USA

aivry@ieee.org samuele.cornell@ieee.org swatanab@andrew.cmu.edu

ABSTRACT

Objective assessment of source-separation systems still mismatches subjective human perception, especially when leakage and self-distortion interact. We introduce the Perceptual Separation (PS) and Perceptual Match (PM), the first pair of measures that functionally isolate these two factors. Our intrusive approach begins with generating a bank of fundamental distortions for each reference waveform signal in the mixture. Distortions, references, and their respective system outputs from all sources are then independently encoded by a pre-trained self-supervised learning model. These representations are aggregated and projected onto a manifold via a nonlinear dimensionality reduction technique called diffusion maps, which aligns Euclidean distances on the manifold with dissimilarities of the encoded waveform representations. On this manifold, the PM measures the Mahalanobis distance from each output to its attributed cluster that consists of its reference and distortions embeddings, capturing self-distortion. The PS accounts for the Mahalanobis distance of the output to the attributed and to the closest non-attributed clusters, quantifying leakage. Both measures are differentiable and operate at a resolution as low as 50 frames per second, allowing granular optimization and analysis of self-distortion and leakage for every output channel of the separation system. We further derive, for both measures, deterministic error radius and non-asymptotic, high-probability confidence intervals (CIs). Experiments on English, Spanish, and music mixtures show that compared to 14 alternative measures, the PS and PM nearly always achieve the highest linear correlation coefficients with human mean-opinion scores, reaching as high as 86.36% for speech and 87.21% for music. We observe, at worst, an error radius of 1.39% and a probabilistic 95% CI of 12.21% for these coefficients, which improves reliable and informed evaluation. Using mutual information, we show that the measures strongly complement each other, and more so as their values decrease, suggesting they are jointly more informative as system performance degrades.¹

1 INTRODUCTION

Progress in source-separation heavily depends on reliable perceptual evaluation, but gold-standard human listening tests remain prohibitively costly and time-consuming ITU-T. (1996; 2003; 2018). Consequently, research commonly relies on objective metrics for model development and comparison. However, the most widely adopted metrics conflate two perceptually distinct failure modes: interference from competing talkers and distortion of the target signal. Measures that better isolate these two modes could help close the gap between automatic evaluation and what listeners actually perceive, potentially enabling an accelerated and more trustworthy development of source separation.

Existing measures typically fall into several groups. Signal-to-distortion ratio (SDR), signal-to-interferences ratio (SIR), signal-to-artifacts ratio (SAR) Vincent et al. (2006), scale-invariant SDR (SI-SDR) Le Roux et al. (2019) and alike usually compute ratios between source to various disturbances purely with waveform energy, offering low complexity and widespread adoption. However, even jointly, they cannot tell by design whether an error stems from leakage or self-distortion. Classical

¹Code available at <https://github.com/Amir-Ivry/MAPSS-measures>

intrusive perceptual and intelligibility metrics like the PESQ Rix et al. (2001), STOI Taal et al. (2011) and ESTOI Jensen & Taal (2016) map an entire utterance to a mean-opinion score (MOS) scale using hand-crafted auditory features. Designed preliminary for speech enhancement, they perform well for corrupted noisy-reverberant speech utterances but may not account for leakage, while also lacking to provide access to their inherent granular processing. Learned black-box metrics such as the DNSMOS family Reddy et al. (2022) that are trained end-to-end to predict crowd-sourced MOS, as well as SpeechBERT Tseng et al. (2021) and Sheet-SSQA Huang et al. (2025), have shown promising results on various speech tasks, but do not offer confidence in their decisions. Spectral-distance metrics are interpretable but tend to mask where degradations occur, e.g., the popular Mel-Cepstral Distortion (MCD) Fukada et al. (1992) collapses the spectral envelope into a global value. Even when taking into account a broader set of metrics, e.g., as available in recently developed speech quality assessment toolkits Shi et al. (2024), no existing family of measures can simultaneously disentangle leakage from distortion, offer granular analysis, and provide error estimates for their decisions.

In this paper, we introduce the Perceptual Separation (PS) and Perceptual Match (PM), the first measures for source separation that functionally disentangle leakage and self-distortion. For every reference frame, at a 50 and 10 frames-per-second rate for speech and music mixtures, respectively, we synthesize a bank of fundamental distortions motivated by psycho-acoustic and auditory theory Gabrielsson & Sjögren (1979); Jekosch (2004); Wilson & Fazenda (2014); Bannister et al. (2024). Then, a pretrained self-supervised model, e.g., wav2vec 2.0 Baevski et al. (2020), is used to independently encode the waveform of references, distortions, and system outputs across all sources, producing high-dimensional frame-wise representations. These are aggregated and projected via diffusion maps Coifman & Lafon (2006) onto a low-dimensional manifold, where a key property of the diffusion maps ensures that Euclidean distances on this manifold align with dissimilarities between encoded representations. Harnessing this property and the geometric structures that distortions form around their references on the manifold, then the Mahalanobis distance from an output embedding to its own cluster is used to calculate the PM, whereas PS also accounts for the distance to the nearest foreign cluster. Because these manifolds are learned at tens of milliseconds resolution, low PS pinpoints cross-talk frames, while low PM isolates self-distortion, indicating actionable debugging cues. We derive theoretical deterministic error radius and non-asymptotic, high-probability confidence intervals (CIs) for both measures. These bounds enable frame-level guarantees on the reliability of the measures.

Evaluated on the SEBASS database Kastner & Herre (2022) that includes mixtures of English, Spanish, and music, the PS and PM jointly deliver the top linear correlation coefficients with subjective mean-opinion scores (MOS) in nearly every scenario, compared with 14 competing widely-used measures. Specifically, coefficients reach as high as 87.21% in music mixtures and 86.36% in English mixtures, with maximal error radius of 1.39% and 95% CI of 12.21%. We also achieve the highest ranking-based correlation coefficients in music mixtures with a maximum of 85.54%, but scoring 84.69% and 83.41% in English and Spanish places the measures in the top-3 and top-5 places, respectively, with an error radius of 0.4% and a 95% CI of 30.03% at worst. These error margins are imperative to an informed and reliable development of more progressed source-separation systems. Empirically, we also show that the normalized mutual information between the measures never exceeds 0.2, and that as their values decrease it approaches zero. This raises the possibility that when the performance of the system degrades, the simultaneous information from both measures becomes more informative for a reliable assessment.

2 PROBLEM FORMULATION

We mark column vectors and matrices with bold symbols and the rest with non-bold symbols.

Consider a trial with index l in which a source separation system with index q performs inference on a single-channel mixture, which includes N^l time frames where at least two speakers are active Vincent et al. (2018). Let \mathcal{F}^l be the set containing these time frame indices, and assume that in time frame $f \in \mathcal{F}^l$ there are $N_f^l \geq 2$ active speakers and their indices are contained in the set \mathcal{S}_f^l . It therefore holds that:

$$|\mathcal{F}^l| = N^l, \quad (1)$$

$$|\mathcal{S}_f^l| = N_f^l. \quad (2)$$

Then, we can model the observed mixture as:

$$\mathbf{z}_f^l = \sum_{i \in \mathcal{S}_f^l} \mathbf{y}_{i,f}^l + \mathbf{v}_f, \quad (3)$$

where $\mathbf{z}_f^l = [z_f^l(n-L+1), \dots, z_f^l(n)]^T \in \mathbb{R}^L$, i.e., frame f has L samples and starts and ends in the $n-L+1$ -th and the n -th sample of its signal, respectively. All vectors in the section follow the same structure and notation as \mathbf{z}_f^l . Each $\mathbf{y}_{i,f}^l \in \mathbb{R}^L$ is defined as the reference signal of the i -th source in frame f and holds the exact source instance that is mixed, potentially including reverberation, distortion, noise, or other interference inherent to its original conditions. The term \mathbf{v}_f represents bounded system and environmental interference, assuming statistical independence of the sources. The estimation of $\mathbf{y}_{i,f}^l$ is denoted $\hat{\mathbf{y}}_{i,f}^{q,l} \in \mathbb{R}^L$.

The first contribution of this paper is the introduction of two new intrusive measures to evaluate source-separation systems. For each source index i :

- The perceptual separation (PS) measure quantifies how well $\hat{\mathbf{y}}_{i,f}^{q,l}$ is perceptually separated from all interfering sources $\{\mathbf{y}_{j,f}^l\}_{j \neq i}$.
- The perceptual match (PM) measure quantifies how closely the estimated source $\hat{\mathbf{y}}_{i,f}^{q,l}$ aligns perceptually with its reference $\mathbf{y}_{i,f}^l$.

The second contribution of this paper is the development of theoretical deterministic error radius and non-asymptotic, high-probability confidence intervals for both measures.

3 MAPSS: MANIFOLD-BASED ASSESSMENT OF PERCEPTUAL SPEECH SEPARATION

This section discusses the theoretical framework and practical steps we apply to calculate the PM and PS measures. We temporarily assume a fixed speech separation system and time frame and omit the indices l, q, f unless otherwise specified.

3.1 DIFFUSION MAPS: THEORETICAL FOUNDATIONS

Diffusion maps provide a low-dimensional manifold representation of a set of high-dimensional points, by learning their geometric and structural relationships Coifman & Lafon (2006). Given a set $\mathcal{X} = \{\mathbf{x}_0, \mathbf{x}_1, \dots, \mathbf{x}_{N-1}\}$ of N data points of dimension M , an affinity matrix $\mathbf{K} \in \mathbb{R}^{N \times N}$ is calculated using a Gaussian kernel:

$$\mathbf{K}_{i,j} = \exp\left(-\frac{\|\mathbf{x}_i - \mathbf{x}_j\|_2^2}{\sigma_{\mathbf{K}}^2}\right), \quad (4)$$

where $i, j \in \{0, \dots, N-1\}$ and $\forall i, j : 0 \leq K_{i,j} \leq 1$, and:

$$\sigma_{\mathbf{K}}^2 = \text{median} \left\{ \|\mathbf{x}_i - \mathbf{x}_j\|_2^2 \mid i \neq j \right\}. \quad (5)$$

To account for non-uniform sampling density of points, an α -normalization replaces \mathbf{K} by $\mathbf{K}^{(\alpha)}$:

$$\mathbf{K}_{i,j}^{(\alpha)} = \frac{\mathbf{K}_{i,j}}{(v_i v_j)^\alpha}, \quad (6)$$

where $\alpha \in [0, 1]$ and $v_i = \sum_{j=0}^{N-1} \mathbf{K}_{i,j}$. Define the diagonal degree-matrix $\mathbf{D}^{(\alpha)} \in \mathbb{R}^{N \times N}$, given by:

$$\mathbf{D}^{(\alpha)} = \text{diag} \left(v_0^{(\alpha)}, \dots, v_{N-1}^{(\alpha)} \right), \quad (7)$$

with:

$$v_i^{(\alpha)} = \sum_{j=0}^{N-1} \mathbf{K}_{i,j}^{(\alpha)}, \quad (8)$$

where $\forall i : v_i^{(\alpha)} > 0$ by construction. For readability, we neglect the α notation from now on. The probability transition matrix $\mathbf{P} \in \mathbb{R}^{N \times N}$ on \mathbf{K} can be defined as:

$$\mathbf{P} = \mathbf{D}^{-1} \mathbf{K}. \quad (9)$$

Note \mathbf{P} is row-stochastic, so $\forall i, j : \mathbf{P}_{ij} \geq 0$, $\sum_{j=0}^{N-1} \mathbf{P}_{ij} = 1$. Spectral decomposition on \mathbf{P} reveals a trivial right eigenvector $\mathbf{u}_0 = \mathbf{1} \in \mathbb{R}^N$ with eigenvalue $\lambda_0 = 1$. Remaining eigenvectors $\{\mathbf{u}_\ell\}_{\ell=1}^{N-1}$ are associated with eigenvalues $\{\lambda_\ell\}_{\ell=1}^{N-1}$ ordered as $1 > \lambda_1 \geq \lambda_2 \geq \dots \geq \lambda_{N-1} > 0$, so that:

$$\mathbf{P} \mathbf{u}_\ell = \lambda_\ell \mathbf{u}_\ell. \quad (10)$$

After $t \in \mathbb{Z}^+$ time steps on \mathbf{P} , the diffusion maps embedding of \mathbf{x}_i onto manifold \mathcal{M} is $\Psi_t : \mathcal{X} \rightarrow \mathbb{R}^{N-1}$:

$$\Psi_t(\mathbf{x}_i) = (\lambda_1^t \mathbf{u}_1(i), \lambda_2^t \mathbf{u}_2(i), \dots, \lambda_{N-1}^t \mathbf{u}_{N-1}(i))^T, \quad (11)$$

where $\{\mathbf{u}_\ell\}_{\ell=1}^{N-1}$ are orthonormal with respect to the stationary measure $\boldsymbol{\pi} = [\pi_0, \dots, \pi_{N-1}]^T \in \mathbb{R}^{N \times 1}$ that satisfies:

$$\pi_i = \frac{\mathbf{D}_{ii}}{\sum_{j=0}^{N-1} \mathbf{D}_{jj}}, \quad (12)$$

where $\pi_i \in (0, 1)$. Let $D_t(i, j)$ be the diffusion distance at time step t between two points \mathbf{x}_i and \mathbf{x}_j :

$$D_t^2(i, j) = \sum_{m=0}^{N-1} \frac{(\mathbf{P}_{im}^t - \mathbf{P}_{jm}^t)^2}{\pi_m} \quad (13)$$

where \mathbf{P}_{im}^t denotes the probability of transitioning from node i to node m in t time steps. Intuitively, the diffusion distance measures the similarity between the probability distributions of random walks starting from nodes i and j . A key strength of diffusion maps we utilize is the following equivalence:

$$D_t^2(i, j) = \|\Psi_t(\mathbf{x}_i) - \Psi_t(\mathbf{x}_j)\|_2^2. \quad (14)$$

This equivalence is fundamental to our approach, since it ensures that Euclidean distances on the manifold align with dissimilarities between their matching high-dimensional points.

In practice, the embedding in (11) is truncated to its first d coordinates, with $d < N - 1$. This simple yet effective step reduces noise sensitivity and retains only the most meaningful, dominant geometric structures Nadler et al. (2006). Mapping $\Psi_t : \mathcal{X} \rightarrow \mathbb{R}^d$ onto manifold $\mathcal{M}^{(d)}$ gives:

$$\Psi_t^{(d)}(\mathbf{x}_i) = (\lambda_1^t \mathbf{u}_1(i), \lambda_2^t \mathbf{u}_2(i), \dots, \lambda_d^t \mathbf{u}_d(i))^T. \quad (15)$$

We cut off the spectral content by choosing d as follows, given $\tau \in [0, 1]$:

$$d = \min \left\{ k \in \{1, \dots, N-1\} : \frac{\sum_{\ell=1}^k \lambda_\ell}{\sum_{\ell=1}^{N-1} \lambda_\ell} \geq \tau \right\}, \quad (16)$$

where we set $\tau = 0.99$. Truncating the spectrum to d dimensions breaks the equality in (14), and leads to a truncation error. In App. (A) we derive the expectation and probabilistic tail bound for this truncation error.

3.2 CONSTRUCTING PERCEPTUAL CLUSTERS ON THE MANIFOLD

Let us recall N_f^l from Section 2. Given $i \in \{0, \dots, N_f^l - 1\}$, the waveform reference signal of the i -th source, \mathbf{y}_i , undergoes N_p hand-crafted perceptual distortions detailed in Appendix D. We define the i -th distortion set \mathcal{D}_i as:

$$\mathcal{D}_i = \{\hat{\mathbf{y}}_i, \mathbf{y}_i, \mathbf{y}_{i,1}, \dots, \mathbf{y}_{i,N_p}\}, \quad (17)$$

where $\mathbf{y}_{i,p} \in \mathbb{R}^L$ is the p -th perceptual distortion of \mathbf{y}_i , for $p \in \{1, \dots, N_p\}$. Each waveform in \mathcal{D}_i is independently encoded via a pre-trained self-supervised model, e.g., wav2vec 2.0 Baevski et al. (2020). Let $\Phi : \mathbb{R}^L \rightarrow \mathbb{R}^M$ be this encoding operator, then:

$$\mathbf{x}_{i,p} = \Phi(\mathbf{y}_{i,p}), \quad \mathbf{x}_i = \Phi(\mathbf{y}_i), \quad \hat{\mathbf{x}}_i = \Phi(\hat{\mathbf{y}}_i). \quad (18)$$

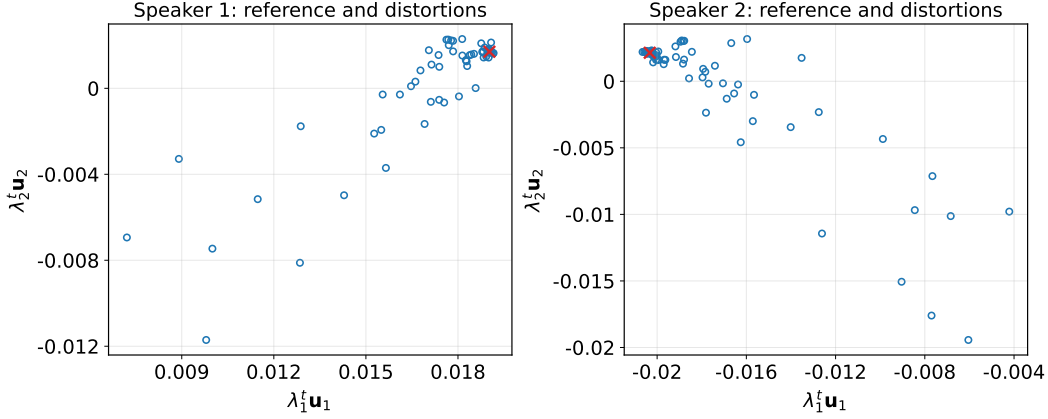


Figure 1: Two embedded clusters on the manifold, associated with a two-speaker English mixture, created via diffusion maps. Each cluster consists of the reference of its speaker denoted by ‘x’ and its distortions marked by circles. We use the two prime coordinates $(\lambda_1^t \mathbf{u}_1, \lambda_2^t \mathbf{u}_2)$ with $t = 1$ (15).

Applying (17), (18) across all N_f^l speech sources, we get the complete high-dimensional dataset:

$$\mathcal{X} = \left\{ \hat{\mathbf{x}}_i, \mathbf{x}_i, \mathbf{x}_{i,1}, \dots, \mathbf{x}_{i,N_p} \mid i = 0, \dots, N_f^l - 1 \right\}, \quad (19)$$

with $|\mathcal{X}| = N_f^l(N_p + 2) := N$. The diffusion maps embedding of $\mathbf{x} \in \mathcal{X}$ on the manifold is thus:

$$\Psi_t^{(d)}(\mathbf{x}) = (\lambda_1^t \mathbf{u}_1(k), \dots, \lambda_d^t \mathbf{u}_d(k))^T \in \mathbb{R}^d, \quad (20)$$

where $k \in \{1, \dots, N\}$ is the global index of \mathbf{x} . We can now define the i -th perceptual cluster on the manifold in the truncated dimension d as:

$$c_i^{(d)} = \left\{ \Psi_t^{(d)}(\mathbf{x}_i), \Psi_t^{(d)}(\mathbf{x}_{i,p}) \mid p = 1, \dots, N_p \right\}. \quad (21)$$

where we exclude the system output embedding $\Psi_t^{(d)}(\hat{\mathbf{x}}_i)$ from $c_i^{(d)}$, since this embedding will be measured against the cluster statistics to yield the PS and PM measures. Including it in the cluster statistics would create circular dependency, where the embedding being evaluated would influence its own evaluation metrics.

By creating a group of waveform distortions from each reference, and then embedding their encoded versions using diffusion maps, perceptual geometric clusters are formed around the references on the manifold, as demonstrated in Figure 1. Crucially, Euclidean distances between each pair of embedded coordinates align with the diffusion distance between their corresponding self-supervised representations (14). We hypothesize and empirically demonstrate that these geometric distances can also be backtracked to perceptual dissimilarity between the corresponding waveforms. This perceptual-geometric correspondence forms the theoretical foundation for our proposed PS and PM measures.

3.3 THE PERCEPTUAL SEPARATION (PS) MEASURE

We aim to quantify the perceptual separation of $\hat{\mathbf{y}}_i$ from its non-attributed references $\{\mathbf{y}_j\}_{i \neq j}$ with the Mahalanobis distance Evans et al. (2021). The empirical centroid and unbiased covariance matrix of the cluster $c_j^{(d)}$ are:

$$\hat{\boldsymbol{\mu}}_j^{(d)} = \frac{1}{|c_j^{(d)}|} \sum_{\boldsymbol{\psi} \in c_j^{(d)}} \boldsymbol{\psi}, \quad (22)$$

$$\hat{\boldsymbol{\Sigma}}_j^{(d)} = \frac{1}{|c_j^{(d)}| - 1} \sum_{\boldsymbol{\psi} \in c_j^{(d)}} \left(\boldsymbol{\psi} - \hat{\boldsymbol{\mu}}_j^{(d)} \right) \left(\boldsymbol{\psi} - \hat{\boldsymbol{\mu}}_j^{(d)} \right)^T, \quad (23)$$

where $\hat{\boldsymbol{\mu}}_j^{(d)} \in \mathbb{R}^d$, $\hat{\boldsymbol{\Sigma}}_j^{(d)} \in \mathbb{R}^{d \times d}$. The Mahalanobis distance from the embedding of the i -th output $\boldsymbol{\Psi}_t^{(d)}(\hat{\mathbf{x}}_i)$ to $c_j^{(d)}$ is given by:

$$d_M \left(\boldsymbol{\Psi}_t^{(d)}(\hat{\mathbf{x}}_i); \hat{\boldsymbol{\mu}}_j^{(d)}, \hat{\boldsymbol{\Sigma}}_j^{(d)} \right) = \sqrt{\left(\boldsymbol{\Psi}_t^{(d)}(\hat{\mathbf{x}}_i) - \hat{\boldsymbol{\mu}}_j^{(d)} \right)^T \left(\hat{\boldsymbol{\Sigma}}_j^{(d)} + \epsilon I^{(d)} \right)^{-1} \left(\boldsymbol{\Psi}_t^{(d)}(\hat{\mathbf{x}}_i) - \hat{\boldsymbol{\mu}}_j^{(d)} \right)}, \quad (24)$$

where we use for regularization $\epsilon = 10^{-6}$ with the d -dimensional identity matrix $I^{(d)}$. We define the measured Mahalanobis distance from $\boldsymbol{\Psi}_t^{(d)}(\hat{\mathbf{x}}_i)$ to its attributed and closest non-attributed clusters as:

$$\hat{A}_i^{(d)} = d_M \left(\boldsymbol{\Psi}_t^{(d)}(\hat{\mathbf{x}}_i); \hat{\boldsymbol{\mu}}_i^{(d)}, \hat{\boldsymbol{\Sigma}}_i^{(d)} \right), \quad (25)$$

$$\hat{B}_i^{(d)} = \min_{j \neq i} d_M \left(\boldsymbol{\Psi}_t^{(d)}(\hat{\mathbf{x}}_i); \hat{\boldsymbol{\mu}}_j^{(d)}, \hat{\boldsymbol{\Sigma}}_j^{(d)} \right), \quad (26)$$

Then, the measured PS score for $\hat{\mathbf{y}}_i$ in the truncated dimension d is:

$$\widehat{\text{PS}}_i^{(d)} = 1 - \frac{\hat{A}_i^{(d)}}{\hat{A}_i^{(d)} + \hat{B}_i^{(d)}}, \quad (27)$$

where higher values are desirable and by design $\hat{A}_i^{(d)} + \hat{B}_i^{(d)} > 0$. The distance to the attributed cluster $\hat{A}_i^{(d)}$ and to the nearest foreign cluster $\hat{B}_i^{(d)}$ balance fidelity and separation, as demonstrated in Figure 2. The PS maintains high values whenever $\hat{A}_i^{(d)} \ll \hat{B}_i^{(d)}$, and falls as $\hat{A}_i^{(d)}$ outgrows $\hat{B}_i^{(d)}$, representing growing leakage when the output of the i -th source in the separation system may perceptually resemble other references more than its attributed one.

Since within each cluster the distribution of distortions may not be isotropic, i.e., some directions capture subtle perturbations while others represent more variable changes, then using Euclidean distance alone would ignore this anisotropy and will not emphasize distortions depending on direction. The Mahalanobis distance resolves this by normalizing with the empirical covariance of each cluster, weighting deviations more heavily in stable directions and less in noisy ones. In this sense, Mahalanobis does not contradict the property (14), it refines it locally and preserves it by incorporating second-order structure of the manifold.

3.4 THE PERCEPTUAL MATCH (PM) MEASURE

The PM measure aims to quantify how perceptually aligned the estimated output $\hat{\mathbf{y}}_i$ is with its reference \mathbf{y}_i . Let $\tilde{c}_i^{(d)} = c_i^{(d)} \setminus \boldsymbol{\Psi}_t^{(d)}(\mathbf{x}_i)$ denote the reference-free i -th cluster. We compute the unbiased empirical covariance matrix of $\tilde{c}_i^{(d)}$, relative to its reference embedding:

$$\hat{\boldsymbol{\Sigma}}_i^{(d)} = \frac{1}{|\tilde{c}_i^{(d)}| - 1} \sum_{\boldsymbol{\psi} \in \tilde{c}_i^{(d)}} \left(\boldsymbol{\psi} - \boldsymbol{\Psi}_t^{(d)}(\mathbf{x}_i) \right) \left(\boldsymbol{\psi} - \boldsymbol{\Psi}_t^{(d)}(\mathbf{x}_i) \right)^T. \quad (28)$$

Then, for $p \in \{1, \dots, N_p\}$ the squared Mahalanobis distance from the p -th distortion to its attributed reference in the i -th cluster, is given by:

$$d_M^2 \left(\boldsymbol{\Psi}_t^{(d)}(\mathbf{x}_{i,p}); \boldsymbol{\Psi}_t^{(d)}(\mathbf{x}_i), \hat{\boldsymbol{\Sigma}}_i^{(d)} \right) = \left(\boldsymbol{\Psi}_t^{(d)}(\mathbf{x}_{i,p}) - \boldsymbol{\Psi}_t^{(d)}(\mathbf{x}_i) \right)^T \left(\hat{\boldsymbol{\Sigma}}_i^{(d)} + \epsilon I^{(d)} \right)^{-1} \left(\boldsymbol{\Psi}_t^{(d)}(\mathbf{x}_{i,p}) - \boldsymbol{\Psi}_t^{(d)}(\mathbf{x}_i) \right), \quad (29)$$

where as in the PS case, $\epsilon = 10^{-6}$. Let us define the set of distances:

$$\hat{\mathcal{G}}_i^{(d)} = \left\{ d_M^2 \left(\boldsymbol{\Psi}_t^{(d)}(\mathbf{x}_{i,p}); \boldsymbol{\Psi}_t^{(d)}(\mathbf{x}_i), \hat{\boldsymbol{\Sigma}}_i^{(d)} \right) \mid p = 1, \dots, N_p \right\}. \quad (30)$$

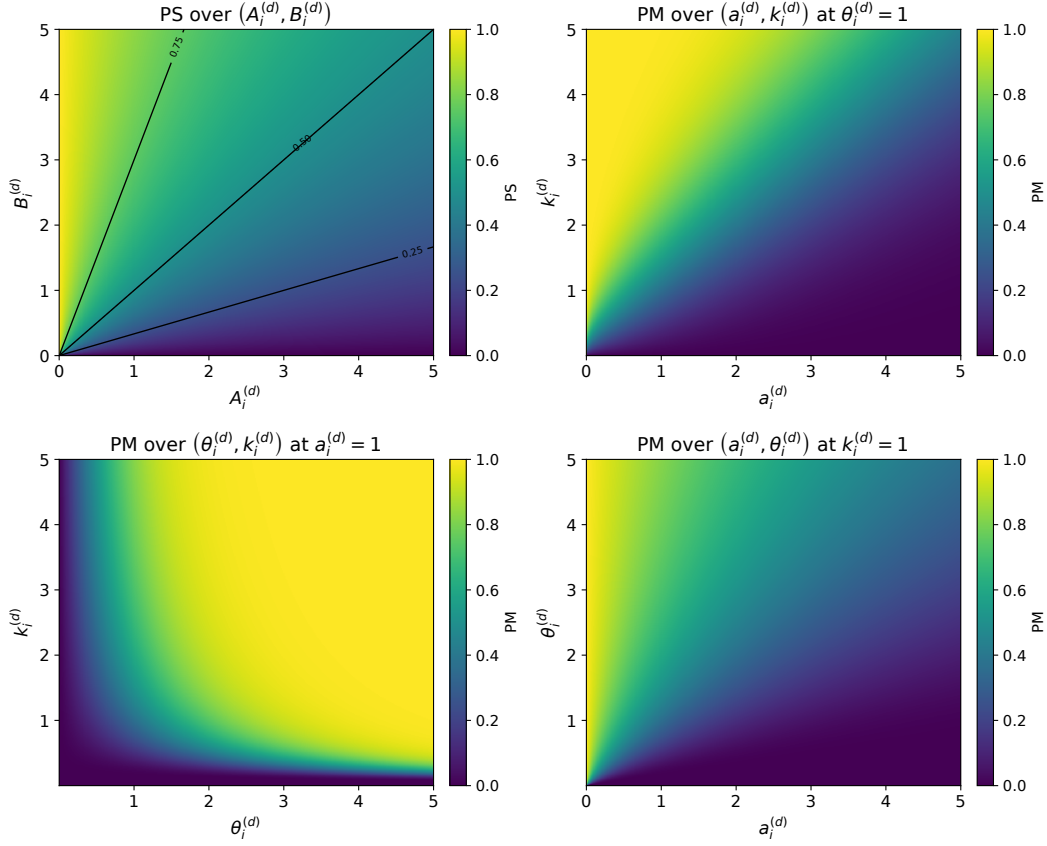


Figure 2: Functional behavior of the PS measure with 0.25, 0.5, 0.75 contour lines, and of the PM measure in three different setups of $\theta_i^{(d)} = 1, a_i^{(d)} = 1, k_i^{(d)} = 1$.

Empirically, we observed that nearly always these distances are well-approximated by a Gamma distribution, validated using Kolmogorov-Smirnov goodness-of-fit tests Kolmogorov (1986); Smirnov (1948). The sample mean and unbiased variance of $\hat{\mathcal{G}}_i^{(d)}$ are estimated by:

$$\hat{\mu}_{\mathcal{G}_i^{(d)}} = \frac{1}{|\hat{\mathcal{G}}_i^{(d)}|} \sum_{g \in \hat{\mathcal{G}}_i^{(d)}} g, \quad (31)$$

$$\hat{\sigma}_{\mathcal{G}_i^{(d)}}^2 = \frac{1}{|\hat{\mathcal{G}}_i^{(d)}| - 1} \sum_{g \in \hat{\mathcal{G}}_i^{(d)}} (g - \hat{\mu}_{\mathcal{G}_i^{(d)}})^2, \quad (32)$$

and can be moment-matched with a Gamma distribution, assuming $\hat{\mu}_{\mathcal{G}_i^{(d)}}, \hat{\sigma}_{\mathcal{G}_i^{(d)}}^2 > 0$, with parameters:

$$\hat{k}_i^{(d)} = \frac{\hat{\mu}_{\mathcal{G}_i^{(d)}}^2}{\hat{\sigma}_{\mathcal{G}_i^{(d)}}^2}, \quad (33)$$

$$\hat{\theta}_i^{(d)} = \frac{\hat{\sigma}_{\mathcal{G}_i^{(d)}}^2}{\hat{\mu}_{\mathcal{G}_i^{(d)}}}. \quad (34)$$

Similarly, the squared Mahalanobis distance from the output embedding to its attributed cluster is:

$$d_M^2 \left(\Psi_t^{(d)}(\hat{\mathbf{x}}_i); \Psi_t^{(d)}(\mathbf{x}_i), \hat{\Sigma}_i^{(d)} \right) := \hat{a}_i^{(d)}. \quad (35)$$

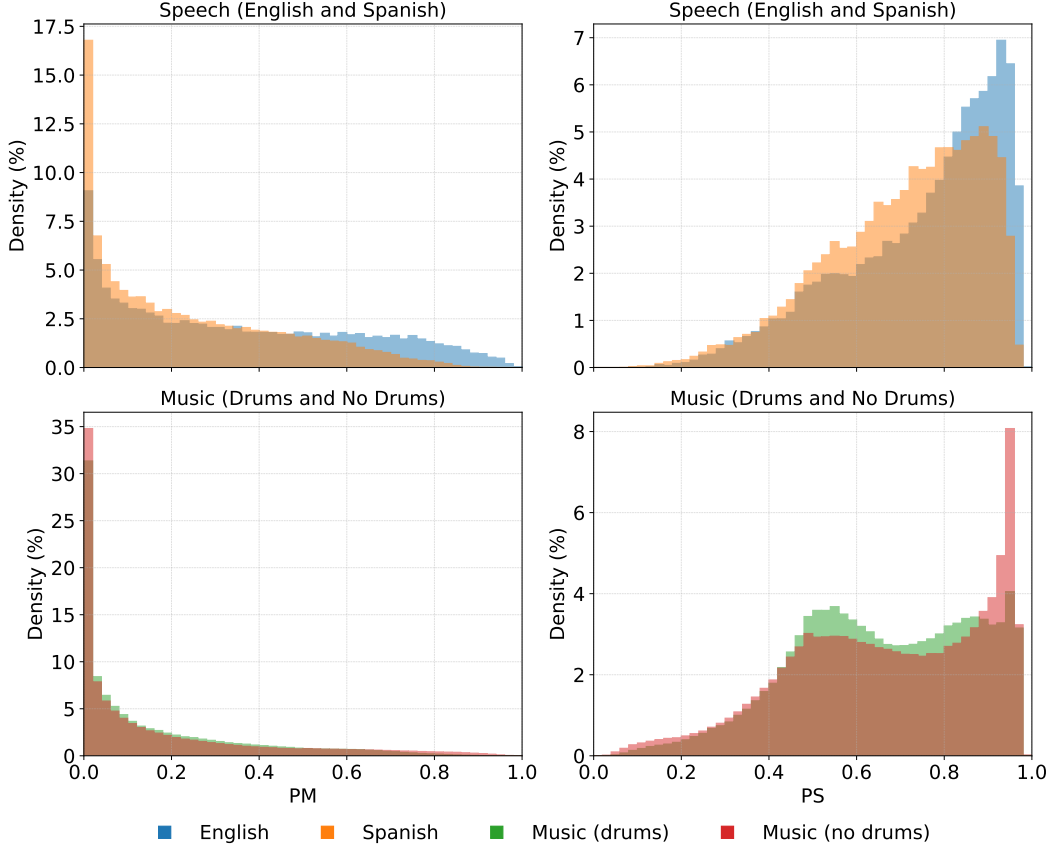


Figure 3: The distribution of PM and PS values across speech and music scenarios from the SEBASS database.

Consider $Q(k, x) = \Gamma(k, x)/\Gamma(k)$ as the regularized upper incomplete Gamma function. Then, the PM score for $\hat{\mathbf{y}}_i$ in dimension d is:

$$\widehat{\text{PM}}_i^{(d)} = Q\left(\hat{k}_i^{(d)}, \frac{\hat{a}_i^{(d)}}{\hat{\theta}_i^{(d)}}\right), \quad (36)$$

where again a higher score is more desirable, and $\hat{k}_i^{(d)}$ and $\hat{\theta}_i^{(d)}$ are well-defined by design as long as $N_p \geq 1$.

Differently from the PS, here the focus shifts to whether an output remains perceptually close to its own reference. Since each cluster of distortions around a reference may be anisotropic, the Mahalanobis distance is again the natural choice. If the output lies well within the bulk of its distortion cluster, the Gamma-tail probability is near one, which may indicate a strong perceptual match. As the output drifts away, the score decays smoothly toward zero, reflecting degradation. Observing Figure 2, in edge cases, when distortions are tightly concentrated, even small mismatches in $a_i^{(d)}$ lower PM sharply, while, when distortions are more broadly dispersed, the PM remains tolerant to larger deviations.

The empirical distributions of the frame-level values of the measures are shown in Figure 3. The PM and PS metrics exhibit contrasting distribution patterns. PM values cluster predominantly around zero with minimal density near one, while PS concentrate near one with virtually no occurrence near zero. Although frame-level human speech quality ratings are not publicly available for direct comparison, these patterns raise comparisons to how humans might perceive audio disturbances. The PM distribution aligns intuitively with human perception, as listeners typically penalize speech quality severely when disturbances occur, making ratings near the scale minimum unsurprising.

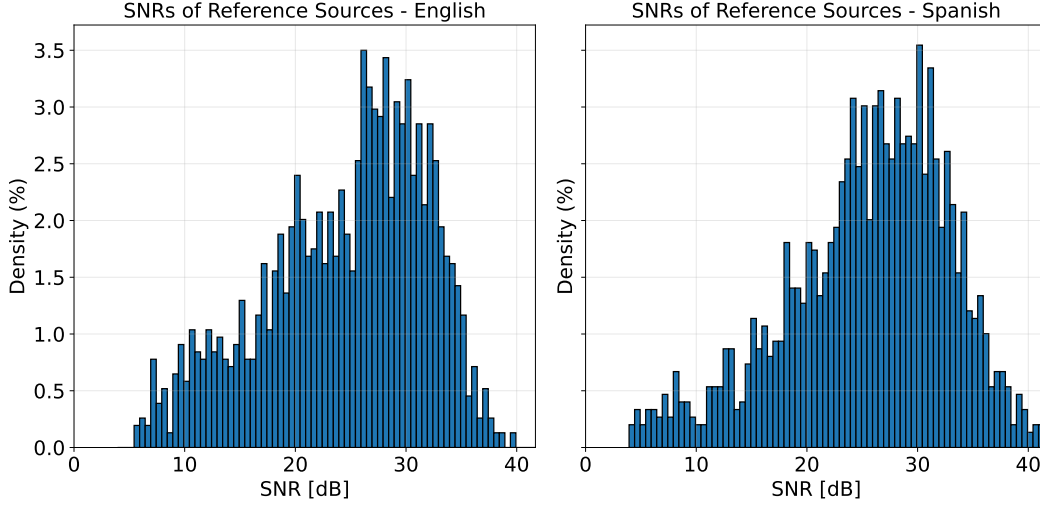


Figure 4: Frame-level SNR estimations for English and Spanish references in the SEBASS database.

However, real granular human ratings would likely show less extreme clustering around zero due to perceptual and rating scale complexities. The PS behavior presents a more complex interpretative challenge. Previous research suggests that humans perceive leakage as more quality-degrading than self-distortions, particularly in acoustic echo cancellation contexts Khanagha et al. (2024), yet our findings here do not support this hypothesis. Whether this discrepancy stems from dataset characteristics, limitations of the PS measure itself, or the mismatch between granular PS values and aggregated human ratings remains unclear and warrants future investigation beyond the scope of this study.

4 EXPERIMENTAL SETUP

4.1 DATABASE

To benchmark the proposed measures, we rely on the Subjective Evaluation of Blind Audio Source Separation (SEBASS) database (Kastner & Herre, 2022), a publicly-available collection of expertly curated listening tests that pools 11,000 individual human ratings for more than 900 separated signals, originating from five evaluation campaigns. SEBASS focuses on distinct scenarios of speech mixtures of 4 male and 4 female speakers, separately, with a pair of English and pair of Spanish speakers in each, and music with both a drums and a no-drums subset, each containing 3 music sources. The split between music mixtures with and without drums is crucial, as percussion transients introduce masking patterns that are perceptually and algorithmically distinct from purely harmonic content, thereby stressing leakage and self-distortion behaviors that do not appear in speech mixtures.

Every mixture was fed to 32 different speech separation systems, spanning classic methods such as non-negative matrix factorization (NMF), spatial filtering and modern deep-learning models. Every output utterance of 10 s, sampled at a sampling frequency of 16 kHz, was judged by 10 or more predominantly certified human raters according to the MUSHRA standard Schoeffler et al. (2018). Every rater was asked to provide a grade between 0 and 100 to the question “grade the basic audio quality of the items under test with respect to the reference signal. Any perceived differences between the reference and the other signal must be interpreted as an impairment”. During grading, the user was exposed to the reference as a baseline and to the hidden reference and mixture anchor as comparative outputs. Figure 4 shows that the speech reference signals have been recorded in a relatively clean environment with signal-to-noise-ratios (SNRs) between 3.9 dB to 41.7 dB, with an average of 25 dB.

The SEBASS dataset suits this study for several reasons. Multilingual coverage of English and Spanish validates language-agnostic behavior, while music tests robustness to highly transient material. Large algorithmic spread creates rich output clusters that stress-test our methodology, and the dense sampling of raters allows for a more reliable estimation of the true mean-opinion score of

subjective human opinion. Importantly, SEBASS represents the only available dataset incorporating human quality ratings for source separation tasks. While creating an additional human-rated dataset falls beyond our scope, we would like to note that expanded perceptual data for source separation would significantly benefit and foster future research in this area.

4.2 PRE-PROCESSING

We first recognize that English and Spanish speakers rarely participate in the same conversation in real-life scenarios. Thus, we separate each 4-speaker mixture into their English and Spanish speakers, creating for each language two mixtures where the one has a pair of male speakers and the other a pair of female speakers. We acknowledge the bias this contributes, as residuals of English may be present in the output signal of a Spanish speaker, and vice versa. It should be mentioned that listening tests have rendered this cross-language leakage extremely negligible, since as expected, source separation systems are able to leverage languages as a meaningful feature to recognize leakage and remove it.

Every waveform, including references, distortions, and outputs from all sources of the mixture, undergoes independent loudness normalization. We use the EBU Recommendation R-128 European Broadcasting Union (EBU) (2011) and set the target level of each waveform to loudness units relative to full scale (LUFS) of -23. If the peak magnitude of the scaled waveform exceeds one, we attenuate it to avoid digital clipping. This step removes loudness bias, known to wrongly affect both human and algorithmic quality judgments, while preserving inter-speaker level relations across the outputs. Since the PS and PM measures address source separation, we also filter out any frames in which there are not at least two active sources using energy-based thresholding.

When applying diffusion maps, we set $\alpha = 1$ in equation (6) to eliminate density-dependent bias from the embedding. This choice ensures that the PS and PM measures reflect the intrinsic geometric structure of the manifold rather than sampling density variations, which would introduce instead artificial distortions into the representation. In the specific case of music with drums, however, we choose to make an exception because density encodes naturally occurring frequency and perceptual salience of transient states, as in drum mixing. Letting $\alpha = 0$ retains density bias and makes the PS and PM event-weighted, which we assume aligns with the perceptual experience of the average human listener. We set $t = 1$ (11) across the board, to keep the diffusion operator focused on local neighborhoods and not being blurred by multi-step mixing.

Unfortunately, granular subjective human scores are not available to the best of our knowledge, although a protocol to obtain them has been established Hansen & Kollmeier (1999). In fact, for source separation, SEBASS provides these scores at utterance-level resolution of approximately 10 seconds. Since our PM and PS measures operate at finer temporal resolutions of 50 and 10 frames-per-second for speech and music, respectively, then aggregation from frame-level to utterance-level is necessary to compare our measure to human MOS. Based on the characteristic of each measure, we have decided to apply average aggregation for the PM and a more perceptual, PESQ-inspired aggregation for the PS.

We now retrieve the indices used in Section 2 to formalize these aggregations. At trial l , let us denote the PM value of the i -th output of source-separation system q in time frame f as $\text{PM}_{i,f}^{q,l}$. We denote $\mathcal{F}_i^l \in \mathcal{F}^l$ as the subset of time-frame indices in which the i -th source is active. Then, the utterance-level PM measure after average aggregation is given by:

$$\text{PM}_{i,\text{utt}}^{q,l} = \frac{1}{|\mathcal{F}_i^l|} \sum_{f \in \mathcal{F}_i^l} \text{PM}_{i,f}^{q,l}. \quad (37)$$

Although average aggregation assumes that human listeners perceive global audio quality by weighing local events equally, which is evidently not the case Rix et al. (2001), we chose to carry it for the PM since its behavior already exhibits strong and frequent granular penalties where the score drops to around zero. Thus, it is assumed that standard human behavior that weighs negative experience heavily in the utterance-level score is implicitly carried out by the nature of the PM measure itself.

However, this is not the case for the PS measure. Here, the aggregation we applied is inspired by the window-based pooling and logistic mapping used inside PESQ Rix et al. (2001). Again, considering only time frame indices in \mathcal{F}_i^l and dropping the rest, let us consider a window of size W frames that

Measure	Scenario	α (6)	t (11)	Aggregation
PS	English	1	1	PESQ
PM	English	1	1	Average
PS	Spanish	1	1	PESQ
PM	Spanish	1	1	Average
PS	Music (no drums)	1	1	PESQ
PM	Music (no drums)	1	1	Average
PS	Music (drums)	0	1	PESQ
PM	Music (drums)	0	1	Average

Table 1: The parameters we pre-defined across scenarios for the PS and PM measures.

slides across the PS measure with a hop size of H frames. Using the p -norm, we define the following:

$$\ell_{i,m}^{q,l} = \left(\frac{1}{W} \sum_{w=1}^W \left| \text{PS}_{i,(m-1)H+w}^{q,l} \right|^p \right)^{1/p}, \quad (38)$$

where $m \in \{1, \dots, M_i^l\}$ and M_i^l is the number of possible windows:

$$M_i^l = \max \left(1, \left\lfloor \frac{|\mathcal{F}_i^l| - W}{H} \right\rfloor \right). \quad (39)$$

We then calculate the following root mean square expression:

$$\ell_i^{q,l} = \sqrt{\frac{1}{M_i^l} \sum_{m=1}^{M_i^l} \left(\ell_{i,m}^{q,l} \right)^2}, \quad (40)$$

and eventually the aggregated PS measure is given by:

$$\text{PS}_{i,\text{utt}}^{q,l} = 0.999 + \frac{4}{1 + \exp(-1.3669 \ell_i^{q,l} + 3.8224)}, \quad (41)$$

where the constants were chosen according to ITU-T (2007). Here, we penalize lower scores explicitly using the p -norm to better match human perceptual aggregation.

The parameters we used for different scenarios and measures are summarized in Table 1.

4.3 METRICS

The preliminary approach we use to evaluate the PM and PS measures is the correlation between their aggregated, utterance-level values and the MOS of the human listeners given in the SEBASS database, which are also utterance-based. We report on two types of correlation coefficients.

At trial l , let the utterance-level MOS of the i -th output from separation system q be $v_i^{q,l}$. Given Q independent source separation systems such that $q \in \{1, \dots, Q\}$, consider the Q -dimensional vectors:

$$\mathbf{PS}_{i,\text{utt}}^l = \left(\text{PS}_{i,\text{utt}}^{1,l}, \dots, \text{PS}_{i,\text{utt}}^{Q,l} \right)^T, \quad (42)$$

$$\mathbf{PM}_{i,\text{utt}}^l = \left(\text{PM}_{i,\text{utt}}^{1,l}, \dots, \text{PM}_{i,\text{utt}}^{Q,l} \right)^T, \quad (43)$$

$$\mathbf{v}_i^l = \left(v_i^{1,l}, \dots, v_i^{Q,l} \right)^T. \quad (44)$$

Pearson product-moment correlation coefficient (PCC) assumes a linear relationship and therefore captures both rank and spacing between paired observations. High PCC indicates that the metric not only orders systems correctly but also preserves the perceptual distance listeners

perceive Benesty et al. (2009). The PCC is measured twice, for the PS and the PM, as follows:

$$r_i^{\text{pcc},l}(\mathbf{PS}_{i,\text{utt}}^l, \mathbf{v}_i^l) = \frac{(\overline{\mathbf{PS}}_{i,\text{utt}}^l)^T \overline{\mathbf{v}}_i^l}{\|\overline{\mathbf{PS}}_{i,\text{utt}}^l\|_2 \|\overline{\mathbf{v}}_i^l\|_2}, \quad (45)$$

$$r_i^{\text{pcc},l}(\mathbf{PM}_{i,\text{utt}}^l, \mathbf{v}_i^l) = \frac{(\overline{\mathbf{PM}}_{i,\text{utt}}^l)^T \overline{\mathbf{v}}_i^l}{\|\overline{\mathbf{PM}}_{i,\text{utt}}^l\|_2 \|\overline{\mathbf{v}}_i^l\|_2}, \quad (46)$$

where $\overline{\mathbf{PS}}_{i,\text{utt}}^l$, $\overline{\mathbf{PM}}_{i,\text{utt}}^l$ and $\overline{\mathbf{v}}_i^l$ are the centered versions of $\mathbf{PS}_{i,\text{utt}}^l$, $\mathbf{PM}_{i,\text{utt}}^l$ and \mathbf{v}_i^l , respectively.

The Spearman rank-order correlation coefficient (SRCC) measures the strength of any monotonic relationship between two variables. Because it depends only on rank, SRCC is insensitive to strictly increasing, possibly non-linear re-scalings of either variable, making it ideal for answering the question “do the PS and PM measures rank systems exactly as listeners do?” Sedgwick (2014). Let $\mathcal{R} : \mathbb{R}^Q \rightarrow R^Q$ be the ranking operator, which in the presence of ties assigns the average ranks. Again, the SRCC is measured for the PS and the PM:

$$\rho_i^{\text{srcc},l}(\mathbf{PS}_{i,\text{utt}}^l, \mathbf{v}_i^l) = r_i^{\text{pcc},l}(\mathcal{R}(\mathbf{PS}_{i,\text{utt}}^l), \mathcal{R}(\mathbf{v}_i^l)), \quad (47)$$

$$\rho_i^{\text{srcc},l}(\mathbf{PM}_{i,\text{utt}}^l, \mathbf{v}_i^l) = r_i^{\text{pcc},l}(\mathcal{R}(\mathbf{PM}_{i,\text{utt}}^l), \mathcal{R}(\mathbf{v}_i^l)). \quad (48)$$

We report these correlation coefficients per English, Spanish, and music mixtures scenarios separately. Given a scenario, we assume that it contains \mathcal{L} independent trials such that $l \in \{1, \dots, \mathcal{L}\}$ with N_{max}^l speakers in each, where:

$$N_{\text{max}}^l = \max_{f \in \mathcal{F}^l} N_f^l. \quad (49)$$

Then, for the PS and PM measures, the PCC and SRCC we report per scenario are given by:

$$\text{PS}^{\text{pcc}} = \frac{1}{\sum_{l=1}^{\mathcal{L}} N_{\text{max}}^l} \sum_{l=1}^{\mathcal{L}} \sum_{i=1}^{N_{\text{max}}^l} r_i^{\text{pcc},l}(\mathbf{PS}_{i,\text{utt}}^l, \mathbf{v}_i^l), \quad (50)$$

$$\text{PM}^{\text{pcc}} = \frac{1}{\sum_{l=1}^{\mathcal{L}} N_{\text{max}}^l} \sum_{l=1}^{\mathcal{L}} \sum_{i=1}^{N_{\text{max}}^l} r_i^{\text{pcc},l}(\mathbf{PM}_{i,\text{utt}}^l, \mathbf{v}_i^l), \quad (51)$$

$$\text{PS}^{\text{srcc}} = \frac{1}{\sum_{l=1}^{\mathcal{L}} N_{\text{max}}^l} \sum_{l=1}^{\mathcal{L}} \sum_{i=1}^{N_{\text{max}}^l} \rho_i^{\text{srcc},l}(\mathbf{PS}_{i,\text{utt}}^l, \mathbf{v}_i^l), \quad (52)$$

$$\text{PM}^{\text{srcc}} = \frac{1}{\sum_{l=1}^{\mathcal{L}} N_{\text{max}}^l} \sum_{l=1}^{\mathcal{L}} \sum_{i=1}^{N_{\text{max}}^l} \rho_i^{\text{srcc},l}(\mathbf{PM}_{i,\text{utt}}^l, \mathbf{v}_i^l). \quad (53)$$

Architecture	Checkpoint	Scenario	Trans. Layers
WavLM Large	microsoft/wavlm-large	English	24
WavLM Base	microsoft/wavlm-base	English	12
Wav2Vec 2.0 Large	facebook/wav2vec2-large-lv60	English	24
Wav2Vec 2.0 Base	facebook/wav2vec2-base	English	12
HuBERT Large	facebook/hubert-large-ls960	English	24
HuBERT Base	facebook/hubert-base-ls960	English	12
Wav2Vec 2.0 Large	facebook/wav2vec2-large-xlsr-53	Spanish	24
AST	MIT/ast-finetuned-audioset-10-10-0.4593	Music	12

Table 2: Self-supervised architectures, their pre-trained checkpoints, scenarios, and number of transformer layers.

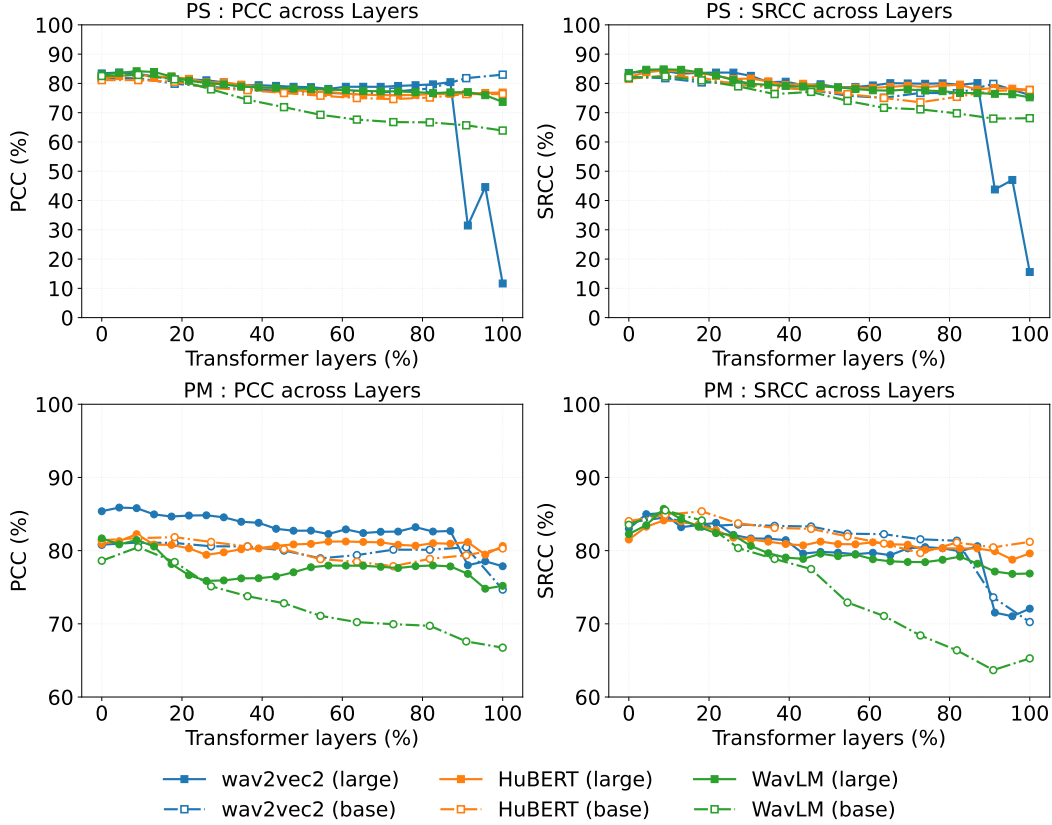


Figure 5: For English mixtures, the effect of transformer layers in different pretrained self-supervised models on the PCC and SRCC values for the PS and PM measures.

5 EXPERIMENTAL RESULTS

All results in this section are derived with zero-shot inference on the entire SEBASS database as described in Section 4, i.e., no training was involved and no data-driven parameter selection was applied.

We begin by analyzing how performance depends on the choice of the pre-trained self-supervised model, the purpose of which is encoding waveforms into perceptual representations before they are fed into the diffusion maps. Table 2 lists the models we examine in this study. We consider six different models for English mixtures, based on the Wav2Vec 2.0 Baevski et al. (2020), WavLM Chen et al. (2022), and HuBERT Hsu et al. (2021) backbones, with Figure 5 demonstrating their layer-wise performance. When using “Large” versions of the models, for both PCC and SRCC values, earlier

Measure	Representation	Transformer Layer	SRCC	PCC
PS	Wav2Vec 2.0 (Large)	2	84.12%	83.74%
PS	Wav2Vec 2.0 (Base)	2	84.25%	83.23%
PM	Wav2Vec 2.0 (Large)	2	84.69%	86.36%
PM	Wav2Vec 2.0 (Base)	2	82.79%	80.07%
PS	WavLM (Large)	3	84.80%	84.16%
PS	WavLM (Base)	2	84.84%	84.19%
PM	WavLM (Large)	3	85.71%	81.44%
PM	WavLM (Base)	2	82.82%	77.51%
PS	HuBERT (Large)	3	84.48%	83.09%
PS	HuBERT (Base)	2	84.83%	82.73%
PM	HuBERT (Large)	3	84.12%	82.24%
PM	HuBERT (Base)	2	81.37%	79.47%
PS	Waveform (raw)	-	73.42%	71.04%
PM	Waveform (raw)	-	69.30%	66.62%

Table 3: For English mixtures, comparing PCC and SRCC values between best-layer performance of “Large” and “Base” models. A raw waveform option, i.e. no encoding, is also reported. The highest SRCC and PCC are in bold per PS and PM.

layers frequently produce representations that allow superior results that gradually decline toward deeper layers, showing approximately 10% average absolute degradation between extremes. Existing layer-wise analysis already reported that acoustic and phonetic content is richly represented in intermediate layers, while deeper layers shift toward semantic abstraction Pasad et al. (2022); Vaidya & Kell (2022). Additional work confirms that distortion sensitivity peaks in the lower or middle layers and diminishes in deeper ones Tamm et al. (2023); Hung et al. (2022), and that pretrained models tend to lose low-level signal fidelity in their deepest layers Moussa & Toneva (2025). A notable data point appears in the final layers of Wav2Vec 2.0 with a sharp drop in performance, especially for PS. This is likely due to its contrastive learning pretraining objective, which drives later layers to specialize in predicting quantized latent codes rather than preserving acoustic detail. For the “Base” versions of the models, we observe a somewhat different behavior. At low and middle layers, their performance is often quite competitive with the “Large” variants, and in several cases the former even outperforms the latter in deeper layers. However, for WavLM, the gap widens toward the final layers, with the “Large” version consistently outperforming. Interestingly, Wav2Vec 2.0 Base does not exhibit the sharp degradation observed in its counterpart and instead its deeper layers remain stable and even show improvements for PS, suggesting that the absence of over-specialization to quantized prediction in the “Base” model preserves sensitivity to perceptual distortions.

Table 3 narrows these models down to their top performing layer, chosen by the max-min criteria of the PCC and SRCC values, across all layers. A no-encoding option is also reported, where waveforms are skip-connected directly into the diffusion maps, which under-performs compared to encoded modes and emphasizes the effectiveness of the waveform encoding in the proposed pipeline. These results reaffirm that shallow layers achieve optimal performance. Although point-by-point comparisons show that “Base” models perform comparably to, or occasionally slightly exceed “Large” models, applying the max-min criteria across the models in the table reveals that “Large” models are preferable when jointly optimizing for PS and PM. For once, Wav2Vec 2.0 Large achieves for the PM a PCC and SRCC differences from its “Base” counterpart of absolute 6% and 2%, respectively, even when the PS case shows a negligible gap. Among the “Large” model variants, Wav2Vec 2.0 Large with transformer layer 2 emerges as the ideal configuration and we carry it forward as a case study we investigate. It should be noted that among “Large” models, the PS very slightly changes with roughly 1% and 0.5% gaps between extremes for the PCC and SRCC, respectively, while the PM gaps are more meaningful. This suggests that the choice of model will mainly affect the PM scores.

In Appendix E, Figure 10 shows reference and output spectrograms from an English mixture, time-aligned to corresponding PM and PS values over a 10-second utterance using the “Large” models, with layers specified in Table 3. While a single example cannot be over-interpreted, the latest observation about the PS gaps across layers is visually supported here, with very similar behavior of all models. The PM shows highly correlated behavior, but with noticeable different values by Wav2Vec 2.0, which exhibits the highest PM value for PCC. An interesting visual example is shown

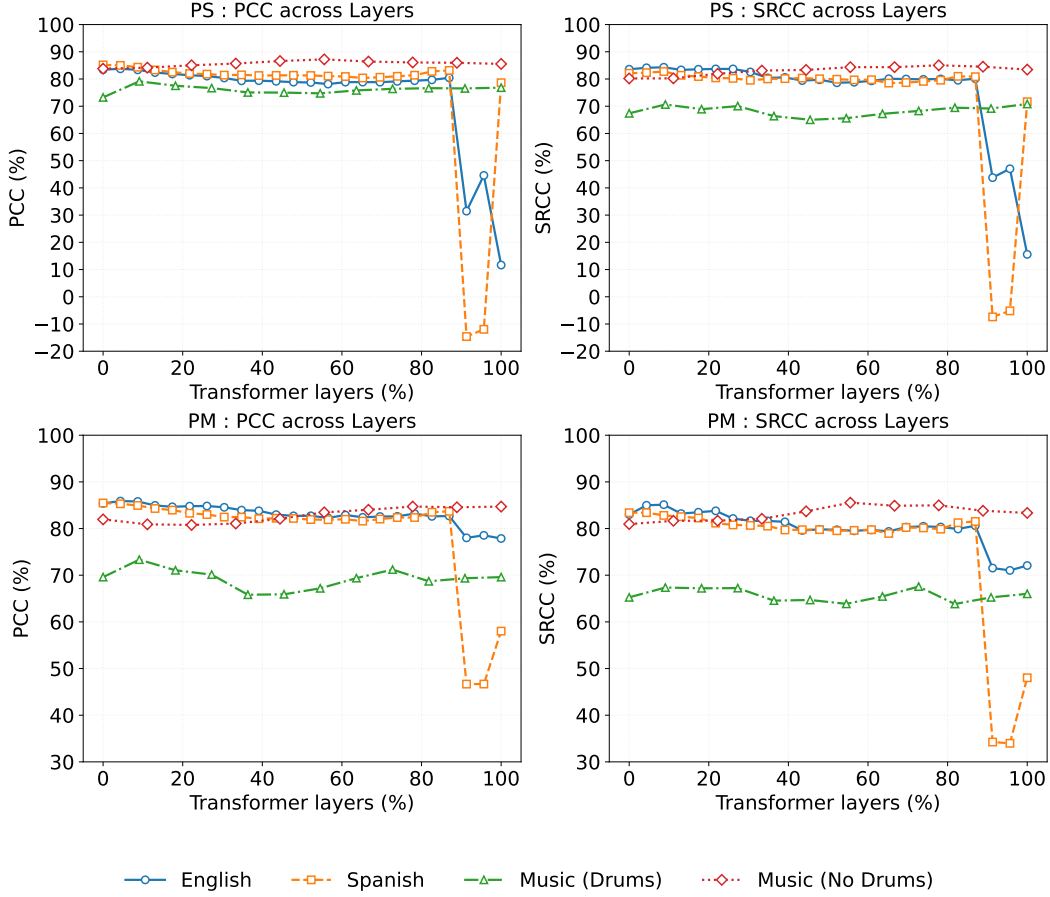


Figure 6: For all scenarios, the effect of transformer layers in their respective pretrained self-supervised architectures on the PCC and SRCC values for the PS and PM measures.

at approximately the 9 seconds mark, when both speakers exhibit visible self-distortion artifacts accompanied by sharp drops in their PM measures. Listening tests confirmed that leakage is indeed more present in “Speaker 2” than in “Speaker 1”, as supported by the PS plot.

Next, we extend the layer-wise analysis to Spanish and music mixtures and compare them with all “Large” English models in Figure 6. Spanish and English mixtures, both evaluated with Wav2Vec 2.0 backbones, show broadly similar trends across layers, but Spanish exhibits a sharper decline in deeper layers. This can be explained by the XLSR pretraining data being relatively scarcer in Spanish than in English, leading later layers to emphasize cross-lingual abstractions over fine acoustic detail Conneau et al. (2020). Music mixtures with drums exhibit the lowest performance among scenarios, which we attribute to the dominance of strong percussive transients. Self-supervised models have demonstrated less stability in these highly non-stationary regions, reducing the ability of PS and PM to capture perceptual degradations Zeghidour et al. (2021). In contrast, music mixtures without drums demonstrate consistently high performance, in some layers even surpassing speech mixtures. This likely stems from the AST backbone being particularly suited in capturing harmonic and timbral structure, allowing the measures to remain faithful to perceptual cues such as instrument texture and vocal clarity Gong et al. (2021). Interestingly, mixtures with drums exhibit reduced performance in the middle layers, while both shallow and deep layers achieve relatively higher coefficients. No-drum mixtures, however, show a relatively flat trend across layers, with a modest peak around the mid-layer region. This suggests that the AST representations of percussive onsets are more vulnerable to degradation in intermediate processing stages. The max-min criteria across all layers, per scenario, shows that the ideal layers for Spanish, drums, and no-drums music mixtures are layers 2, 2, and 6, respectively. As for English, we carry these ideal configurations forward.

Measure	English		Spanish		Music (Drums)		Music (No Drums)	
	SRCC	PCC	SRCC	PCC	SRCC	PCC	SRCC	PCC
PS	84.12%	83.74%	82.33%	85.01%	70.63%	79.14%	84.35%	87.21%
PM	84.69%	86.36%	83.41%	85.30%	67.35%	73.33%	85.54%	83.47%
PS (waveform)	73.42%	71.04%	74.69%	75.05%	51.75%	61.83%	78.88%	78.95%
PM (waveform)	69.30%	66.62%	68.27%	67.35%	49.52%	51.77%	74.37%	75.51%
STOI	80.85%	78.40%	78.79%	82.56%	67.29%	71.27%	75.64%	78.13%
eSTOI	82.14%	82.28%	79.20%	82.68%	54.68%	57.35%	70.06%	74.45%
PESQ	85.56%	84.05%	86.06%	84.98%	61.60%	53.87%	61.26%	60.24%
SI-SDR	78.11%	76.96%	84.07%	81.38%	42.08%	56.98%	70.42%	71.96%
SDR	77.72%	73.13%	84.29%	76.07%	44.78%	54.33%	74.51%	75.35%
SIR	51.28%	56.20%	45.67%	55.19%	18.64%	35.76%	51.00%	55.12%
SAR	75.54%	72.98%	78.21%	73.29%	36.98%	40.81%	66.15%	68.96%
CI-SDR	78.66%	77.41%	84.32%	81.48%	45.02%	55.42%	74.25%	75.11%
DNSMOS-OVRL	63.70%	67.77%	35.34%	43.57%	21.79%	34.27%	13.81%	19.47%
MCD	43.05%	33.86%	45.90%	37.97%	30.27%	42.23%	33.49%	32.19%
SpeechBERT	68.58%	67.44%	69.55%	70.48%	52.33%	59.71%	75.60%	81.13%
Sheet-SSQA	41.17%	51.38%	61.06%	73.01%	39.40%	29.03%	14.19%	5.17%
UTMOS	55.53%	55.43%	52.22%	55.75%	-9.24%	-8.25%	12.59%	7.72%
NISQA	60.78%	67.62%	63.37%	66.58%	27.27%	41.73%	42.33%	48.07%

Table 4: SRCC and PCC of the PS and PM measures (underlined), their waveform counterparts, and 14 comparative measures, across scenarios. The top-3 results in every column are in bold.

Table 4 benchmarks the proposed PS and PM measures against 14 established metrics for speech and audio quality and also versus its waveform-only version. Per scenario, we report our measures with the best-performing configuration. For English mixtures, both PS and PM consistently lead the table, except for PESQ taking the top with SRCC higher by an absolute of roughly 1% than our measures. The advantage of PESQ in rank correlation can be attributed to its long-standing perceptual model, which explicitly encodes aspects of loudness perception, asymmetry, and time-alignment penalties, features that directly penalize separation artifacts. In Spanish mixtures, PS and PM maintain top performance in terms of PCC, but fall behind PESQ and SDR-based metrics in SRCC. One possible explanation is that the syllable-timed rhythm and steady vowels of Spanish make fidelity-driven metrics such as SI-SDR, CI-SDR, and SDR more predictive of listener rankings, as these metrics emphasize reconstruction accuracy at the waveform level. For music mixtures, PS and PM achieve the strongest overall correlations across both drums and no-drums conditions. Even though SpeechBERTscore has shown impressive results and is also based on a self-supervised backbone, it is mostly not competitive with our measures, and notably even performing worse than our raw waveform version at times, which projects on the importance of the diffusion maps in the pipeline. We emphasize that unlike English, we only inspected one backbone model for Spanish or music mixtures. Also, the average and PESQ-like aggregation strategies were not a data-driven optimization but rather an heuristic and reasoning-based choice. Consequently, while the proposed measures already demonstrate strong alignment with human perception, these low-hanging fruits may potentially boost performance. Quite surprisingly, the first group of STOI, PESQ, and SDR-based measures is consistently preferable to the second group consisting of DNSMOS, speechBERTscore, UTMOS, and others, which rarely achieve more than 70% in performance. One crucial conclusion this table suggests is that measures originally developed for a certain audio application, should not be zero-shot adapted into other applications, and in that case into source separation evaluation. Otherwise, there is a realistic risk of reporting values that highly drift from human opinion, and that may spiral the development of audio technologies instead of accelerating it. Ultimately, the PM and PS results suggest a strong validation of them as the superior choices to capture leakage and self-distortion in a manner that resonates with human judgments for source separation systems.

An additional stress test for our measures concerns their robustness to temporal misalignment between the input and output streams of the separator, a phenomenon commonly introduced by modern communication systems or, e.g., when dealing with references obtained from different, per-speaker microphones, such as in meeting datasets Carletta et al. (2005); Vinnikov et al. (2024). Figure 7 illustrates the effect of artificial delays ranging from 0 ms to 100 ms across English, Spanish, and music scenarios. While performance gradually degrades for speech scenarios as misalignment

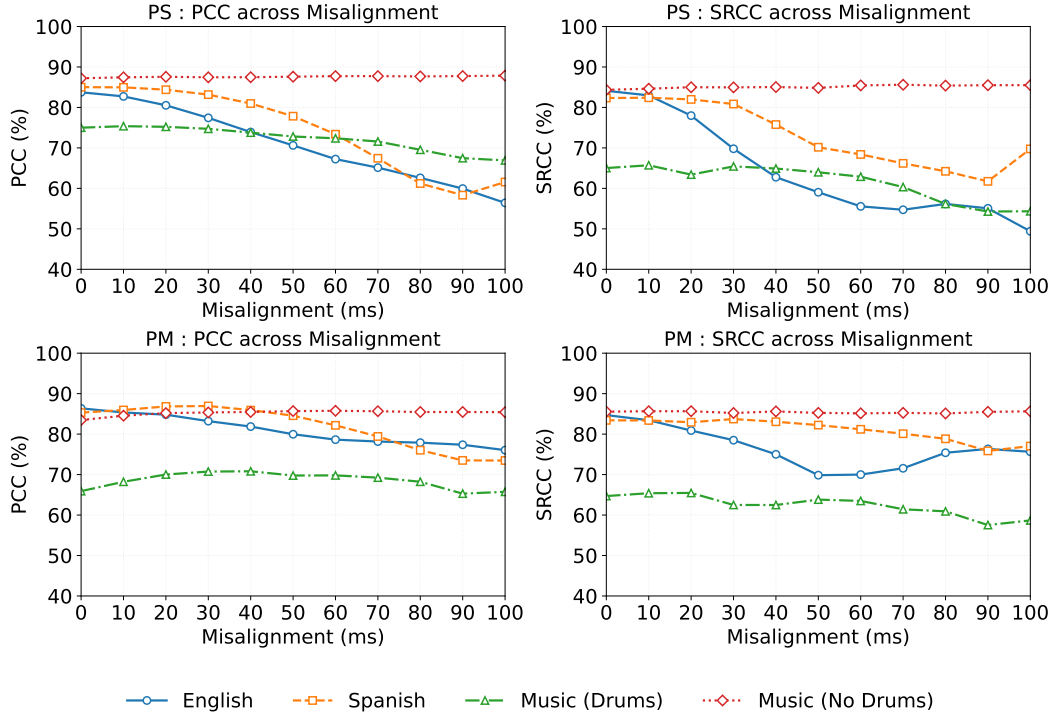


Figure 7: The effect of temporal misalignment between references and outputs of the separation system on the PS and PM measures.

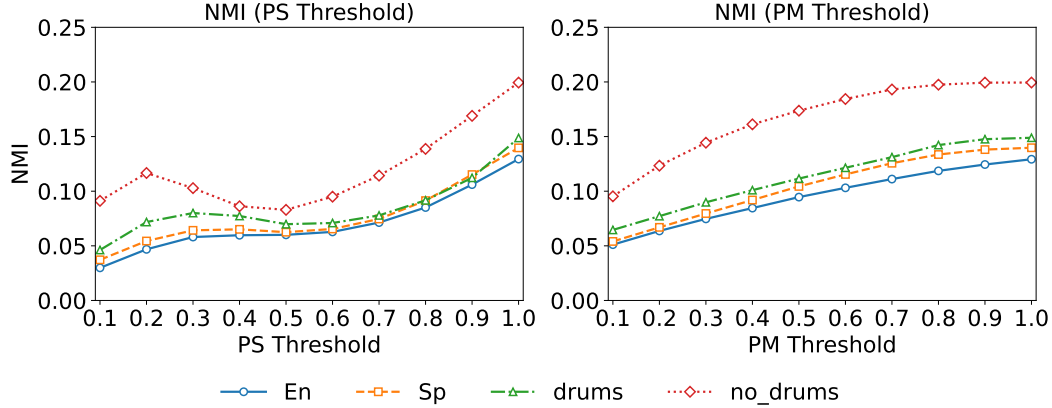


Figure 8: Normalized mutual information between the PS and PM measures across their thresholded values.

grows, as expected, a 20 ms delay or less still preserves coefficients higher than 80%. Surpassing this threshold, however, often causes a pronounced drop that underscores this weakness in our measures, since human ratings are insensitive to these short latencies. Music mixtures exhibit a different pattern, as performance remains largely stable across delays, with the presence of drums introducing more variability than its counterpart. This robustness can be partly attributed to the Audio Spectrogram Transformer (AST), which processes music with a temporal resolution of 100 ms and a receptive field of 160 ms, making it inherently less sensitive to short misalignments at the cost of reduced granularity.

We examine the complementary relationship between PS and PM using normalized mutual information (NMI) Danon et al. (2005), which captures instantaneous statistical dependence beyond linear

effects, where a lower NMI indicates less shared information. Each measure is first normalized per utterance to the range $[0, 1]$. Then, for a threshold in the set $\{0.1, 0.2, \dots, 1\}$, we retain frames with PS values lower than the threshold, and compute the NMI between the aligned pairs of the PS and PM, aggregated across utterances and conditions. We repeat the procedure with roles reversed, i.e., thresholding on the PM. As shown in Figure 8, NMI is generally modest and tends to decrease as the threshold tightens, approaching near-zero at the extreme. This pattern suggests that PS and PM convey increasingly complementary information when source separation quality is poor. Conversely, at looser thresholds, NMI rises up to 0.2. Since NMI can reach 1 under full redundancy, however, even this upper bound still indicates a considerable degree of complementarity between the measures. These results support reporting both PS and PM, particularly in challenging conditions, since each measure captures failure modes that the other may miss. For transparency, we also report the number of samples contributing to each threshold that was used in the NMI estimates in Table 7 in Appendix F.

In the next phase, we investigate the deterministic error radius and probabilistic CIs derived for the PS and PM measures in Appendix B. Figure 9 shows histograms of the frame-level error distributions for speech and music mixtures. As expected, the radius caused by the spectral truncation in the diffusion maps process is typically an order of magnitude smaller than the 95% probabilistic width, originated from finite-sample clusters on the manifold. The error radius is also concentrated mostly near zero, which further confirms its negligibility. CIs typically span 10-50% of the dynamic range of the measures at the frame level, but surprisingly in the PM, between 10-15% of frame-level instances have probabilistic tails that approach zero across scenarios. The immediate contribution of these results are by making development of source separation systems more reliable and informed at the frame-level.

Now, we investigate how these frame-level errors propagate into the reported PCC and SRCC values at the scenario level, following the methodology detailed in Appendix C. The resulting deterministic and probabilistic error ingredients are summarized in Table 5. The former never exceeding 1.39%, a bias that even in the worst case barely changes the performance ranking in Table 4. A more critical finding concerns the latter. To reach 95% confidence in the reported coefficients, PM requires at most an additional 8.98% margin, while PS requires as much as 30.03%. This difference shows a trade-off where PS provides valuable sensitivity to source leakage but carries higher statistical uncertainty when propagated to scenario-level correlation coefficients. The practical consequences are twofold. First, while both measures align well with human perception, PM should be viewed as statistically more robust, particularly when system differences are small. Second, the larger confidence requirements for PS suggest that it should be used primarily as a complementary diagnostic, capturing perceptual aspects not reflected in PM but at the cost of greater variability. This complementarity underscores the value of considering PS and PM jointly, i.e., PS reveals perceptual distortions that may otherwise be missed, while PM ensures the stability and reliability of the reported correlations.

Finally, to give the reader an intuitive grasp of how the two error terms evolve in a time-aligned manner with the PS and PM measures, Figure 11 in Appendix E illustrates a representative example.

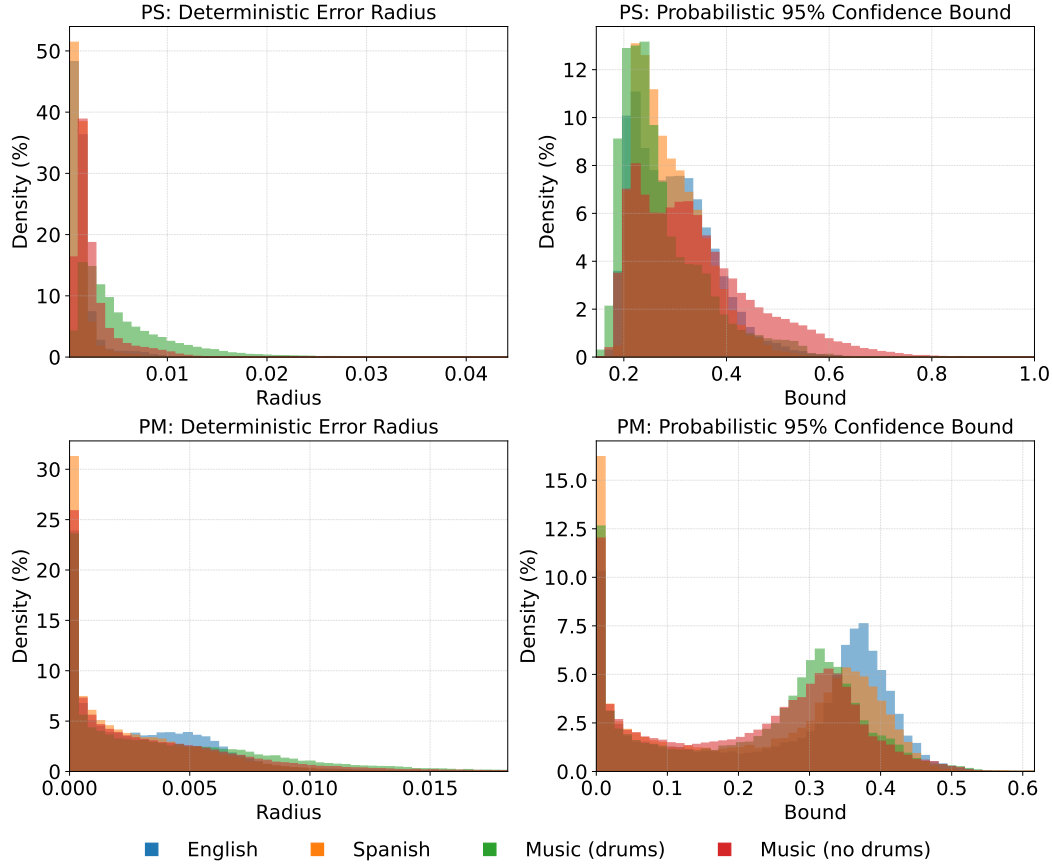


Figure 9: An histogram view of the frame-level deterministic error radius and the 95% probabilistic tail in the PS and PM measures across scenarios.

	SRCC	PCC
PS radius	0.16%	0.21%
PS tail (95%)	30.03%	10.29%
PM radius	0.11%	0.99%
PM tail (95%)	7.23%	3.83%

(a) English

	SRCC	PCC
PS radius	0.10%	0.14%
PS tail (95%)	26.39%	8.85%
PM radius	0.18%	1.23%
PM tail (95%)	8.98%	4.28%

(b) Spanish

	SRCC	PCC
PS radius	0.40%	0.72%
PS tail (95%)	28.71%	12.21%
PM radius	0.29%	1.39%
PM tail (95%)	6.25%	4.15%

(c) Music (Drums)

	SRCC	PCC
PS radius	0.14%	0.11%
PS tail (95%)	12.69%	4.11%
PM radius	0.02%	1.04%
PM tail (95%)	4.75%	1.77%

(d) Music (No Drums)

Table 5: The deterministic error radius and probabilistic tail with 95% confidence of the PCC and SRCC values, across scenarios.

6 LIMITATIONS

Several factors currently limit the broad applicability of the PS and PM measures.

Our validation depends exclusively on the SEBASS database, the only public corpus that provides human ratings for source separation systems. This corpus does not support variation of languages, accents, recording conditions, or speaker configurations that enables statistically significant conclusions across these verticals. Moreover, the listening tests used to collect human ratings ask a generic basic quality question, rather than questions that isolate leakage versus self-distortion. This design choice may attenuate the ground-truth sensitivity to the specific error modes that PS and PM are intended to disentangle, and can introduce a systematic bias that even multi-rater averaging cannot fully cancel. Another noticeable limitation of this research concerns the aggregation techniques we employ to convert frame-level to utterance-level scores. Since neither granular human ratings exist nor is there any documented data-driven mapping from granular to global human ratings, we limit the capability of the PS and PM measures by merely approximating aggregation functions. In future work we aim to collect and release the first source separation benchmark that incorporates diverse realistic scenarios and granular human subjective ratings with targeted questions for leakage and self-distortions.

On a single NVIDIA A6000 GPU paired with 32 CPU cores with 64 GB of memory, our implementation achieves a real-time factor of 1.2, e.g., when analyzing a 25 ms frame in 30 ms on average. While this enables offline evaluation and hyper-parameter sweeps, it falls short of strict real-time monitoring and may limit large-scale neural-architecture searches and limit using the PS and PM measures inside loss function during training sessions. Profiling reveals that the dominant bottlenecks are diffusion-map eigendecompositions and repeated Mahalanobis distance computations with per-frame covariance estimation for all distortions points in every cluster. We plan to introduce more efficient implementations as we maintain our code repository.

We also point out that in music mixtures, 0.5% of frames exhibit for the PM measure an error radius that exceeds 1, rendering these observations irrelevant. These cases should be ignored completely, and future work that focuses on the separation of music sources will further investigate this phenomenon.

7 CONCLUSIONS

To evaluate source separation systems more reliably and consistently, we introduce the PS and PM, a pair of frame-level differentiable measures that assess leakage and self-distortion on a diffusion map manifold using Mahalanobis geometry. Beyond proposing the measures, we established deterministic error envelopes and non-asymptotic confidence intervals, making the scores not only informative but also actionable under quantified uncertainty. Validations across English, Spanish, and music mixtures show that PM and PS correlate more strongly with human mean-opinion scores than existing alternative measures in the majority of tested scenarios. Moreover, it is suggested that as system quality degrades, the more mutual information increases between the measures, indicating that their joint use provides the most diagnostic value.

Looking ahead, we expect this two-fold view to streamline development in three concrete ways. First, as a diagnostic lens, PS and PM can pinpoint whether errors arise from target distortion or cross-talk, accelerating ablation, data curation, and model selection. Second, as training-time guidance, their differentiability enables loss shaping or curriculum triggers that explicitly trade fidelity against separation while monitoring confidence. Third, as a benchmarking layer, the attached uncertainty bounds support fairer hyper-parameter sweeps and reporting practices.

REFERENCES

- Radosław Adamczak. A note on the Hanson–Wright inequality for random vectors with dependencies. *Electronic Journal of Probability*, 20:1–13, 2015. doi: 10.1214/EJP.v20-3412.
- Alexei Baevski, Henry Zhou, Abdelrahman Mohamed, and Michael Auli. wav2vec 2.0: A framework for self-supervised learning of speech representations. In *Advances in Neural Information Processing Systems*, volume 33, pp. 12449–12460, 2020.
- Scott Bannister, Alinka E. Greasley, Trevor J. Cox, Michael A. Akeroyd, Jon Barker, Bruno Fazenda, Jennifer Firth, Simone N. Graetzer, Gerardo Roa Dabike, Rebecca R. Vos, et al. Muddy, muddled, or muffled? understanding the perception of audio quality in music by hearing aid users. *Frontiers in Psychology*, 15:1310176, 2024.
- Maurice S. Bartlett. On the theoretical specification and sampling properties of autocorrelated time-series. *Supplement to the Journal of the Royal Statistical Society*, 8(1):27–41, 1946. doi: 10.2307/2983611. URL <https://www.jstor.org/stable/2983611>.
- Jacob Benesty, Jingdong Chen, Yiteng Huang, and Israel Cohen. Pearson correlation coefficient. In *Noise reduction in speech processing*, pp. 1–4. Springer, 2009.
- Jean Carletta, Simone Ashby, Sebastien Bourban, Mike Flynn, Mael Guillemot, Thomas Hain, Jaroslav Kadlec, Vasilis Karaiskos, Wessel Kraaij, Melissa Kronenthal, et al. The ami meeting corpus: A pre-announcement. In *International workshop on machine learning for multimodal interaction*, pp. 28–39. Springer, 2005.
- Sanyuan Chen, Chengyi Wang, Zhengyang Chen, Yu Wu, Shujie Liu, Zhuo Chen, Jinyu Li, Naoyuki Kanda, Takuya Yoshioka, Xiong Xiao, Jian Wu, Long Zhou, Shuo Ren, Yanmin Qian, Yao Qian, Jian Wu, Michael Zeng, and Furu Wei. WavLM: Large-scale self-supervised pre-training for full stack speech processing. *IEEE Journal of Selected Topics in Signal Processing*, 16(6):1505–1518, 2022. doi: 10.1109/JSTSP.2022.3187672.
- Ronald R. Coifman and Stéphane Lafon. Diffusion maps. *Applied and computational harmonic analysis*, 21(1):5–30, 2006.
- Alexis Conneau, Alexei Baevski, Ronan Collobert, Abdelrahman Mohamed, and Michael Auli. Unsupervised cross-lingual representation learning for speech recognition. *arXiv preprint arXiv:2006.13979*, 2020.
- Leon Danon, Albert Díaz-Guilera, Jordi Duch, and Alex Arenas. Comparing community structure identification. *Journal of Statistical Mechanics: Theory and Experiment*, 2005(09):P09008, 2005. doi: 10.1088/1742-5468/2005/09/P09008. Introduced the normalized mutual information measure for evaluating clustering similarity in networks.
- Bradley Efron and Robert J. Tibshirani. *An Introduction to the Bootstrap*, volume 57 of *Monographs on Statistics and Applied Probability*. Chapman& Hall/CRC, New York, 1994. ISBN 9780412042317.
- European Broadcasting Union (EBU). EBU recommendation R128: Loudness normalisation and permitted maximum level of audio signals. Technical recommendation, European Broadcasting Union, Geneva, Switzerland, 2011. URL <https://tech.ebu.ch/docs/r/r128.pdf>. Originally issued August 2010; revised 2011.
- Luke Evans, Maria K. Cameron, and Pratyush Tiwary. Computing committors in collective variables via mahalanobis diffusion maps. *arXiv preprint arXiv:2108.08979*, Aug 2021.
- Toshiaki Fukada, Keiichi Tokuda, Takao Kobayashi, and Satoshi Imai. An adaptive algorithm for mel-cepstral analysis of speech. In *ICASSP*, volume 92, pp. 137–140, 1992.
- Alf Gabrielsson and Håkan Sjögren. Perceived sound quality of sound-reproducing systems. *The Journal of the Acoustical Society of America*, 65(4):1019–1033, 1979.
- Yuan Gong, Yu-An Chung, and James Glass. AST: Audio spectrogram transformer. In *Proceedings of Interspeech*, 2021.

- Martin Hansen and Birger Kollmeier. Continuous assessment of time-varying speech quality. *The Journal of the Acoustical Society of America*, 106(5):2888–2899, 1999. doi: 10.1121/1.428116.
- Matthias Hein, Jean-Yves Audibert, and Ulrike von Luxburg. From graphs to manifolds – weak and strong pointwise consistency of graph laplacians. In *COLT*, volume 3559 of *Lecture Notes in Computer Science*, pp. 470–485. Springer, 2005. URL https://doi.org/10.1007/11503415_32.
- Roger A. Horn and Charles R. Johnson. *Matrix Analysis*. Cambridge University Press, Cambridge, UK, 2nd edition, 2013. ISBN 9781107033413.
- Wei-Ning Hsu, Benjamin Bolte, Yao-Hung Hubert Tsai, Kushal Lakhota, Ruslan Salakhutdinov, and Abdelrahman Mohamed. HuBERT: Self-supervised speech representation learning by masked prediction of hidden units. *IEEE/ACM Transactions on Audio, Speech, and Language Processing*, 29:3451–3460, 2021. doi: 10.1109/TASLP.2021.3122291.
- Wen-Chin Huang, Erica Cooper, and Tomoki Toda. SHEET: A multi-purpose open-source speech human evaluation estimation toolkit. *arXiv preprint arXiv:2505.15061*, 2025.
- Yu-Wen Hung, Szu-Wei Fu Cheng, Yu Tsao, and Hsin-Min Wang. Boosting self-supervised embeddings for speech quality assessment. In *Proceedings of Interspeech*, pp. 2288–2292, 2022.
- ITU-T. ITU-T P.800: Methods for subjective determination of transmission quality. Technical report, Inter. Telecommunication Union, 1996. URL <https://www.itu.int/rec/T-REC-P.800/en>.
- ITU-T. ITU-T P.835: Subjective test methodology for evaluating speech communication systems that include noise suppression algorithm. Technical report, Inter. Telecommunication Union, 2003. URL <https://www.itu.int/rec/T-REC-P.835/en>.
- ITU-T. ITU-T P.862.2: Wideband extension to Recommendation P.862 for the assessment of wideband telephone networks and speech codecs. Recommendation, International Telecommunication Union, Telecommunication Standardization Sector (ITU-T), Geneva, Switzerland, November 2007. URL <https://handle.itu.int/11.1002/1000/9275>.
- ITU-T. ITU-T P.808: Subjective evaluation of speech quality with a crowdsourcing approach. Technical report, Inter. Telecommunication Union, 2018. URL <https://www.itu.int/rec/T-REC-P.808/en>.
- Ute Jekosch. Basic concepts and terms of “quality”, reconsidered in the context of product-sound quality. *Acta Acustica united with Acustica*, 90(6):999–1006, 2004.
- Jesper Jensen and Cees H. Taal. An algorithm for predicting the intelligibility of speech masked by modulated noise maskers. *IEEE/ACM Transactions on Audio, Speech, and Language Processing*, 24(11):2009–2022, 2016. doi: 10.1109/TASLP.2016.2585878.
- Thorsten Kastner and Jürgen Herre. The SEBASS-DB: A consolidated public data base of listening test results for perceptual evaluation of BSS quality measures. In *2022 International Workshop on Acoustic Signal Enhancement (IWAENC)*, pp. 1–5. IEEE, 2022.
- Maurice Kendall and Jean D. Gibbons. *Rank Correlation Methods*. Edward Arnold, London, 5 edition, 1990. ISBN 9780340506326.
- Vahid Khanagha, Dimitrios Koutsaidis, Kshitij Kalgaonkar, and Sridha Srinivasan. Interference Aware Training Target for DNN-based Joint Acoustic Echo Cancellation and Noise Suppression. In *INTERSPEECH*, pp. 1–5. ISCA, 2024. URL https://www.isca-archive.org/interspeech_2024/khanagha24_interspeech.pdf.
- Andrey N. Kolmogorov. On the empirical determination of a distribution law. In Albert N. Shiryaev (ed.), *Selected Works of A. N. Kolmogorov, Volume II*, pp. 139–146. Springer, New York, 1986. English translation of 1933 Italian paper.
- Jonathan Le Roux, Scott Wisdom, Hakan Erdogan, and John R. Hershey. SDR–half-Baked or Well Done? In *ICASSP*, pp. 626–630, 2019.

- Omer Moussa and Mariya Toneva. Brain-tuned speech models better reflect speech processing stages in the brain. *arXiv preprint arXiv:2506.03832*, June 2025. Proceedings of Interspeech 2025.
- Boaz Nadler, Stéphane Lafon, Ronald R Coifman, and Ioannis G Kevrekidis. Diffusion maps, spectral clustering and reaction coordinates of dynamical systems. *Applied and Computational Harmonic Analysis*, 21(1):113–127, 2006.
- Ankita Pasad, Alexei Baevski, Emmanuel Dupoux, and Karen Livescu. Comparative layer-wise analysis of self-supervised speech models. In *Proceedings of Interspeech*, 2022.
- Chandan K. A. Reddy, Vishak Gopal, and Ross Cutler. DNSMOS P.835: A non-intrusive perceptual objective speech quality metric to evaluate noise suppressors. *arXiv preprint arXiv:2110.01763*, 2022.
- Anthony W. Rix, John G. Beerends, Michael P. Hollier, and Andries P. Hekstra. Perceptual evaluation of speech quality (PESQ)—a new method for speech quality assessment of telephone networks and codecs. In *ICASSP*, volume 2, pp. 749–752, 2001.
- Walter Rudin. *Principles of Mathematical Analysis*. International Series in Pure and Applied Mathematics. McGraw–Hill, New York, 3 edition, 1976.
- Michael Schoeffler, Sarah Bartoschek, Fabian-Robert Stoter, Marlene Roess, Susanne Westphal, Bernd Edler, and Jürgen Herre. webMUSHRA - a comprehensive framework for web-based listening tests. *Journal of Open Research Software*, 6(1), 2018.
- Philip Sedgwick. Spearman’s rank correlation coefficient. *BMJ*, 349:g7327, November 28 2014. doi: 10.1136/bmj.g7327.
- Jiatong Shi, Hye-jin Shim, Jinchuan Tian, Siddhant Arora, Haibin Wu, Darius Petermann, Jia Qi Yip, You Zhang, Yuxun Tang, Wangyou Zhang, Dareen Safar Alharthi, Yichen Huang, Koichi Saito, Jionghao Han, Yiwen Zhao, Chris Donahue, and Shinji Watanabe. VERSA: A versatile evaluation toolkit for speech, audio, and music. *arXiv preprint arXiv:2412.17667*, 2024.
- Nikolai V. Smirnov. Table for estimating the goodness of fit of empirical distributions. *The Annals of Mathematical Statistics*, 19(2):279–281, 1948. doi: 10.1214/aoms/1177730256.
- Cees H. Taal, Richard C. Hendriks, Richard Heusdens, and Jesper Jensen. An algorithm for intelligibility prediction of time–frequency weighted noisy speech. *IEEE Trans. Audio, Speech and Language Processing*, 19(7):2125–2136, 2011.
- Lukas Tamm, Sebastian Möller, and Babak Naderi. Layer-wise analysis of xls-r representations for speech quality assessment. *arXiv preprint arXiv:2308.12077*, 2023.
- Wei-Cheng Tseng, Chien-yu Lee, and Hung-yi Lee. SpeechBERT: Cross-modal pre-trained language model for end-to-end spoken question answering. *arXiv preprint arXiv:2104.08203*, 2021.
- Gaurav Vaidya and Alexander J E Kell. Self-supervised models of audio effectively explain human cortical responses to speech. *bioRxiv*, 2022.
- Roman Vershynin. *High-Dimensional Probability: An Introduction with Applications in Data Science*. Cambridge Series in Statistical and Probabilistic Mathematics. Cambridge University Press, 2nd edition, 2024. Second edition, posted May 20 2024. Available online.
- Emmanuel Vincent, R.émi Gribonval, and Cédric Févotte. Performance measurement in blind audio source separation. *IEEE Trans. Audio, Speech and Language Processing*, 14(4):1462–1469, 2006.
- Emmanuel Vincent, Tuomas Virtanen, and Sharon Gannot (eds.). *Audio Source Separation and Speech Enhancement*. Wiley, 2018.
- Alon Vinnikov, Amir Ivry, Aviv Hurvitz, Igor Abramovski, Sharon Koubi, Ilya Gurvich, Shai Pe’er, Xiong Xiao, Benjamin Martinez Elizalde, Naoyuki Kanda, Xiaofei Wang, Shalev Shaer, Stav Yagev, Yossi Asher, Sunit Sivasankaran, Yifan Gong, Min Tang, Huaming Wang, and Eyal Krupka. The NOTSOFAR-1 challenge: New datasets, baseline, and tasks for distant meeting transcription. In *Proc. Interspeech*, pp. 5003–5007, Kos Island, Greece, 2024. doi: 10.21437/Interspeech.2024-1788.

Alex Wilson and Bruno Fazenda. Characterisation of distortion profiles in relation to audio quality. In *DAFx*, pp. 1–8, 2014.

Neil Zeghidour, Nicolas Usunier, Gabriel Synnaeve, and Emmanuel Dupoux. Leaf: A learnable frontend for audio classification. In *Proceedings of ICLR*, 2021.

A EXPECTATION AND PROBABILISTIC CONFIDENCE BOUND OF THE TRUNCATION ERROR

Assume a point $\mathbf{x}_i \in \mathcal{X}$ is drawn from the stationary distribution π (12) of the diffusion process, where $i \in \{1, \dots, N\}$. This assumption is supported by (Hein et al., 2005, Lem. 1), and by showing empirically on 5,000 graphs that the corresponding eigenvector matches the theoretical stationary distribution up to statistical fluctuations. Given that the $N - 1$ -dimensional embedding of \mathbf{x}_i is truncated to dimension d , then the truncation error is expressed as (15):

$$E(\mathbf{x}_i) = \left(\sum_{\ell=d+1}^{N-1} \lambda_\ell^{2t} \mathbf{u}_\ell^2(i) \right)^{1/2}. \quad (54)$$

We define the squared truncation error and analyze it:

$$T(\mathbf{x}_i) = E^2(\mathbf{x}_i) = \sum_{\ell=d+1}^{N-1} \lambda_\ell^{2t} \mathbf{u}_\ell^2(i). \quad (55)$$

Since the eigenvectors $\{\mathbf{u}_\ell\}_{\ell=0}^{N-1}$ are orthonormal under π , then:

$$\mathbb{E}_\pi [\mathbf{u}_\ell^2(i)] = \sum_{i=0}^{N-1} \pi_i \mathbf{u}_\ell^2(i) = 1, \quad (56)$$

from which we derive the expectation of $T(\mathbf{x}_i)$ under π :

$$\mathbb{E}_\pi [T(\mathbf{x}_i)] = \mathbb{E}_\pi \left(\sum_{\ell=d+1}^{N-1} \lambda_\ell^{2t} \mathbf{u}_\ell^2(i) \right) = \sum_{\ell=d+1}^{N-1} \lambda_\ell^{2t}. \quad (57)$$

Thus, the expectation of the truncation error is given directly by:

$$\mathbb{E}_\pi [E(\mathbf{x}_i)] = \left(\sum_{\ell=d+1}^{N-1} \lambda_\ell^{2t} \right)^{1/2}. \quad (58)$$

This term decays monotonically as d grows and is typically lower than 10^{-3} . To obtain a non-asymptotic and high-probability confidence bound on the truncation error, we derive $\forall \ell, i$ (56):

$$|\mathbf{u}_\ell(i)| \leq \pi_{\min}^{-1/2}, \quad \pi_{\min} = \min_{i \in \{1, \dots, N\}} \pi. \quad (59)$$

Any bounded variable is sub-Gaussian, and its ψ_2 -norm is at most the bound divided by $\sqrt{\ln 2}$ (Vershynin, 2024, Example 2.6.5):

$$\|\mathbf{u}_\ell(i)\|_{\psi_2, \pi} \leq \frac{\pi_{\min}^{-1/2}}{\sqrt{\ln 2}} := K. \quad (60)$$

Let $m = N - 1 - d$, so we define $\mathbf{z}_i \in \mathbb{R}^m$ as:

$$\mathbf{z}_i = (\mathbf{u}_{d+1}(i), \dots, \mathbf{u}_{N-1}(i))^T, \quad (61)$$

and the diagonal matrix of weights $\mathbf{D} \in \mathbb{R}^{m \times m}$ as:

$$\mathbf{D} = \text{diag}(\lambda_{d+1}^t, \dots, \lambda_{N-1}^t). \quad (62)$$

Then $E(\mathbf{x}_i)$ and $T(\mathbf{x}_i)$ can be rewritten as:

$$T(\mathbf{x}_i) = \|\mathbf{D}\mathbf{z}_i\|_2^2, \quad (63)$$

$$E(\mathbf{x}_i) = \|\mathbf{D}\mathbf{z}_i\|_2. \quad (64)$$

For $\ell > 0$, $\mathbf{u}_\ell(i)$ is zero-mean under π . Consequently, the vector \mathbf{z}_i is zero-mean and by definition satisfies $\|\mathbf{z}_i\|_{\psi_2, \pi} \leq K\sqrt{m}$. We also notice that multiplication by a fixed matrix scales the sub-Gaussian norm linearly, and since \mathbf{D} is symmetric and positive:

$$\|\mathbf{D}\mathbf{z}(i)\|_{\psi_2, \pi} \leq K\sqrt{m}\|\mathbf{D}\|_2 = K\sqrt{m} \max_{\ell > d} \lambda_\ell^t = K\sqrt{m}\lambda_{d+1}^t. \quad (65)$$

According to (Vershynin, 2024, Prop. 6.2.1), for an m -dimensional, zero-mean and sub-Gaussian vector \mathbf{Y} with $\|\mathbf{Y}\|_{\psi_2, \pi} \leq \kappa$, it holds:

$$\mathbb{P}_{\pi}\{\|\mathbf{Y}\|_2 \geq C\kappa(\sqrt{m} + t)\} \leq e^{-t^2}, \quad (66)$$

where $t \geq 0$ and $C > 0$ is a constant. Setting $\mathbf{Y} = \mathbf{D}\mathbf{z}_i$ and $\kappa = K\sqrt{m}\lambda_{d+1}^t$ gives:

$$\mathbb{P}_{\pi}\left\{T(\mathbf{x}_i) > C^2\lambda_{d+1}^{2t}K^2m(\sqrt{m} + t)^2\right\} \leq e^{-t^2}. \quad (67)$$

Let $\delta \in (0, 1)$ and set $t = \sqrt{\ln(1/\delta)}$. We can rewrite (67) as:

$$\mathbb{P}_{\pi}\left\{T(\mathbf{x}_i) \leq C^2\lambda_{d+1}^{2t}K^2m\left(\sqrt{m} + \sqrt{\ln \frac{1}{\delta}}\right)^2\right\} \geq 1 - \delta. \quad (68)$$

Thus, the desired confidence bound on the truncation error is:

$$\mathbb{P}_{\pi}\left\{E(\mathbf{x}_i) \leq C\lambda_{d+1}^tK\left(m + \sqrt{m \ln \frac{1}{\delta}}\right)\right\} \geq 1 - \delta. \quad (69)$$

The choice of d dimensions affects both m that shrinks linearly with d and λ_{d+1}^t that falls monotonically with d . K is affected by the minimal stationary probability π_{\min} , so if the graph contains rare points then π_{\min} may be tiny, while a well-balanced graph derives $K \sim \sqrt{N}$ and tightens the bound.

B DETERMINISTIC ERROR RADIUS AND PROBABILISTIC TAIL BOUND OF THE MEASURES

We derive a deterministic error radius and a high-probability confidence bound on the frame-level PS and PM measures by considering: (i) spectral truncation error due to retaining d diffusion coordinates; (ii) finite-sample uncertainty in estimating the cluster centroid and covariance. We then combine these via union bounds. In this section, we consider a trial l , system q , and time frame f .

B.1 THE PS MEASURE

Considering source $i, j \in \{0, \dots, N_f^l - 1\}$, we begin by analyzing the effect of the truncation error, assuming access to cluster statistics. The difference between the embedding of $\hat{\mathbf{x}}_i$ and the centroid of cluster j can be expressed in the truncated subspace \mathbb{R}^d and in its complement subspace \mathbb{R}^m , respectively denoted $\Delta_{i,j}^{(d)}$ and $\Delta_{i,j}^{(\perp)}$. Using (15), (22):

$$\Delta_{i,j}^{(d)} = \Psi_t^{(d)}(\hat{\mathbf{x}}_i) - \mu_j^{(d)} \in \mathbb{R}^d, \quad (70)$$

$$\Delta_{i,j}^{(\perp)} = \Psi_t^{(\perp)}(\hat{\mathbf{x}}_i) - \mu_j^{(\perp)} \in \mathbb{R}^m, \quad (71)$$

where $m = N - d - 1$. For completion, for every $\mathbf{x} \in \mathcal{X}$ and its global index $k \in \{1, \dots, N\}$:

$$\mu_j^{(\perp)} = \frac{1}{|c_j^{(\perp)}|} \sum_{\psi \in c_j^{(\perp)}} \psi \quad (72)$$

$$c_j^{(\perp)} = \left\{ \Psi_t^{(\perp)}(\mathbf{x}_j), \Psi_t^{(\perp)}(\mathbf{x}_{j,p}) \mid p = 1, \dots, N_p \right\} \quad (73)$$

$$\Psi_t^{(\perp)}(\mathbf{x}) = (\lambda_{d+1}^t \mathbf{u}_{d+1}(k), \dots, \lambda_{N-1}^t \mathbf{u}_{N-1}(k)). \quad (74)$$

In the full, $N - 1$ -dimensional space, the cluster c_j is given by:

$$c_j = \{ \Psi_t(\mathbf{x}_j), \Psi_t(\mathbf{x}_{j,p}) \mid p = 1, \dots, N_p \}, \quad (75)$$

with mean $\mu \in \mathbb{R}^{N-1}$, difference $\Delta_{i,j} \in \mathbb{R}^{N-1}$ and covariance $\Sigma_j \in \mathbb{R}^{(N-1) \times (N-1)}$ that hold:

$$\mu_j = \begin{bmatrix} \mu_j^{(d)} \\ \mu_j^{(\perp)} \end{bmatrix}, \quad \Delta_{i,j} = \begin{bmatrix} \Delta_{i,j}^{(d)} \\ \Delta_{i,j}^{(\perp)} \end{bmatrix}, \quad \Sigma_j = \begin{bmatrix} \Sigma_j^{(d)} & \mathbf{C}_j \\ \mathbf{C}_j^T & \Sigma_j^{(\perp)} \end{bmatrix}, \quad (76)$$

where $\Sigma_j^{(\perp)} \in \mathbb{R}^{m \times m}$ and $\mathbf{C}_j \in \mathbb{R}^{d \times m}$ are:

$$\Sigma_j^{(\perp)} = \frac{1}{|c_j^{(\perp)}| - 1} \sum_{\psi \in c_j^{(\perp)}} (\psi - \mu_j^{(\perp)}) (\psi - \mu_j^{(\perp)})^T, \quad (77)$$

$$\mathbf{C}_j = \frac{1}{|c_j^{(\perp)}| - 1} \sum_{p=0}^{N_p} \left(\Psi_t^{(d)}(\mathbf{x}_{j,p}) - \mu_j^{(d)} \right) \left(\Psi_t^{(\perp)}(\mathbf{x}_{j,p}) - \mu_j^{(\perp)} \right)^T. \quad (78)$$

According to (24), the squared Mahalanobis distance from $\Psi_t(\hat{\mathbf{x}}_i)$ to c_j is:

$$d_M^2(\Psi_t(\hat{\mathbf{x}}_i); \mu_j, \Sigma_j) = \Delta_{i,j}^T \left(\Sigma_j + \epsilon I^{(N-1)} \right)^{-1} \Delta_{i,j}, \quad (79)$$

where inversion is empirically obtained by taking $\epsilon = 10^{-6}$ with $I^{(N-1)}$ being the $N - 1$ -dimensional identity matrix. To evaluate the truncation effect, we perform blockwise inversion on (79) via the Schur complement Horn & Johnson (2013):

$$d_M^2(\Psi_t(\hat{\mathbf{x}}_i); \mu_j, \Sigma_j) = \left(\Delta_{i,j}^{(d)} \right)^T \left(\Sigma_j^{(d)} + \epsilon I^{(d)} \right)^{-1} \Delta_{i,j}^{(d)} + \mathbf{r}_{i,j}^T \mathbf{S}_j^{-1} \mathbf{r}_{i,j}, \quad (80)$$

where $\mathbf{r}_{i,j} \in \mathbb{R}^m$ and the Schur complement $\mathbf{S}_j \in \mathbb{R}^{m \times m}$ hold:

$$\mathbf{r}_{i,j} = \Delta_{i,j}^{(\perp)} - \mathbf{C}_j^T \left(\Sigma_j^{(d)} + \epsilon I^{(d)} \right)^{-1} \Delta_{i,j}^{(d)}, \quad (81)$$

$$\mathbf{S}_j = \Sigma_j^{(\perp)} - \mathbf{C}_j^T \left(\Sigma_j^{(d)} + \epsilon I^{(d)} \right)^{-1} \mathbf{C}_j. \quad (82)$$

We now utilize the inequality:

$$\forall a, b \geq 0 : \quad \left| \sqrt{a+b} - \sqrt{a} \right| \leq \sqrt{b}, \quad (83)$$

obtained by the mean-value theorem for $f(\cdot) = \sqrt{\cdot}$ (Rudin, 1976, Ch. 5). Let us set:

$$a = \left(\Delta_{i,j}^{(d)} \right)^T \left(\Sigma_j^{(d)} + \epsilon I^{(d)} \right)^{-1} \Delta_{i,j}^{(d)}, \quad (84)$$

$$b = \mathbf{r}_{i,j}^T \mathbf{S}_j^{-1} \mathbf{r}_{i,j}, \quad (85)$$

to obtain:

$$|\delta_{i,j}| = \left| d_M(\Psi_t(\hat{\mathbf{x}}_i); \boldsymbol{\mu}_j, \Sigma_j) - d_M(\Psi_t^{(d)}(\hat{\mathbf{x}}_i); \boldsymbol{\mu}_j^{(d)}, \Sigma_j^{(d)}) \right| \leq \sqrt{\mathbf{r}_{i,j}^T \mathbf{S}_j^{-1} \mathbf{r}_{i,j}}. \quad (86)$$

Namely, $|\delta_{i,j}|$ is the truncation error of this Mahalanobis distance. From (25)-(26), it holds that:

$$\delta_{i,i} = A_i - A_i^{(d)}, \quad \delta_{i,j^*} = B_i - B_i^{(d)}, \quad (87)$$

where:

$$j^* = \arg \min_{j \in \{0, \dots, N_j^l - 1\}, j \neq i} d_M(\Psi_t^{(d)}(\hat{\mathbf{x}}_i); \boldsymbol{\mu}_j^{(d)}, \Sigma_j^{(d)}) \quad (88)$$

$$A_i = d_M(\Psi_t(\hat{\mathbf{x}}_i); \boldsymbol{\mu}_i, \Sigma_i), \quad (89)$$

$$B_i = d_M(\Psi_t(\hat{\mathbf{x}}_i); \boldsymbol{\mu}_{j^*}, \Sigma_{j^*}). \quad (90)$$

Consider the $N - 1$ -dimensional representation of $\text{PS}_i^{(d)}$, i.e. PS_i (27):

$$\text{PS}_i = 1 - \frac{A_i}{A_i + B_i}, \quad (91)$$

which is smooth and differentiable in A_i and B_i , since by definition $A_i + B_i > 0$. We assume and have empirically validated that truncation introduces a small relative change, i.e.:

$$|\delta_{i,i}| \ll A_i^{(d)} + B_i^{(d)}, \quad (92)$$

$$|\delta_{i,j^*}| \ll A_i^{(d)} + B_i^{(d)}, \quad (93)$$

making the first-order Taylor expansion of PS_i around $(A_i^{(d)}, B_i^{(d)})$ valid. We can therefore write:

$$\begin{aligned} \text{PS}_i - \text{PS}_i^{(d)} &\simeq \frac{\partial \text{PS}_i}{\partial A_i} (A_i^{(d)}, B_i^{(d)}) \delta_{i,i} + \frac{\partial \text{PS}_i}{\partial B_i} (A_i^{(d)}, B_i^{(d)}) \delta_{i,j^*} \\ &= -\frac{B_i^{(d)}}{(A_i^{(d)} + B_i^{(d)})^2} \delta_{i,i} + \frac{A_i^{(d)}}{(A_i^{(d)} + B_i^{(d)})^2} \delta_{i,j^*}, \end{aligned} \quad (94)$$

where the quadratic remainder in the expansion is empirically one order smaller than the first-order term and can be safely dropped. Applying the triangle inequality and (86) yields the deterministic error radius in the PS measure:

$$\left| \text{PS}_i - \text{PS}_i^{(d)} \right| \leq \frac{B_i^{(d)} |\delta_{i,i}| + A_i^{(d)} |\delta_{i,j^*}|}{(A_i^{(d)} + B_i^{(d)})^2} = \frac{B_i^{(d)} \sqrt{\mathbf{r}_{i,i}^T \mathbf{S}_i^{-1} \mathbf{r}_{i,i}} + A_i^{(d)} \sqrt{\mathbf{r}_{i,j^*}^T \mathbf{S}_{j^*}^{-1} \mathbf{r}_{i,j^*}}}{(A_i^{(d)} + B_i^{(d)})^2}. \quad (95)$$

We now quantify the uncertainty in $\widehat{\text{PS}}_i^{(d)}$ due to finite-sample cluster statistics. Empirically, we observe that cluster coordinates exhibit weak dependence between one another and derive from Bartlett (1946) the following cut-off rule for the effective sample size of cluster $c_j^{(d)}$:

$$n_{j,\text{eff}} = \frac{n_j}{1 + 2 \sum_{\ell=1}^{L_j} \hat{\rho}_{j,\ell}}, \quad n_j = |c_j^{(d)}| \quad (96)$$

where $\hat{\rho}_{j,\ell}$ is the empirical average Pearson auto-correlation of coordinates at lag ℓ , and:

$$L_j = \arg \min_{\ell} \left\{ |\hat{\rho}_{j,\ell}| < \frac{z_{0.975}}{\sqrt{n_j - \ell}} \right\}. \quad (97)$$

Empirical evidence across 5,000 graphs suggest that on average $\sum_{\ell} \hat{\rho}_{j,\ell} \simeq 0.2$, and so we set $n_{j,\text{eff}} = 0.7 n_j$ for all clusters.

To bound the deviation between the estimated and true cluster mean and covariance, we employ the vector and matrix Bernstein (Vershynin, 2024, Props. 2.8.1, 4.7.1) and the dependent Hanson-Wright inequalities (Adamczak, 2015, Thm. 2.5). For every $\delta_{j,\mu}^{\text{PS}}, \delta_{j,\Sigma}^{\text{PS}} \in (0, 1/2)$, with respective least probabilities $1 - \delta_{j,\mu}^{\text{PS}}$ and $1 - \delta_{j,\Sigma}^{\text{PS}}$:

$$|\mu_j - \hat{\mu}_j| \leq \sqrt{\frac{2\lambda_{\max}(\hat{\Sigma}_j^{(d)}) \ln(2/\delta_{j,\mu}^{\text{PS}})}{n_{j,\text{eff}}}} := \Delta_{j,\mu} \quad (98)$$

$$\|\Sigma_j^{(d)} - \hat{\Sigma}_j^{(d)}\|_2 \leq C\lambda_{\max}(\hat{\Sigma}_j^{(d)}) \left(\frac{r_j}{n_{j,\text{eff}}} + \frac{r_j + \ln(2/\delta_{j,\Sigma}^{\text{PS}})}{n_{j,\text{eff}}} \right) := \Delta_{j,\Sigma}, \quad (99)$$

with an absolute constant $C > 0$ and the ratio:

$$r_j = \frac{\text{tr}(\hat{\Sigma}_j^{(d)})}{\lambda_{\max}(\hat{\Sigma}_j^{(d)})}. \quad (100)$$

Let us integrate the definitions of $\hat{A}_i^{(d)}$ (25) and $\hat{B}_i^{(d)}$ (26) with (98)-(99). Then, with probability of at least $1 - \delta_{i,\mu}^{\text{PS}} - \delta_{i,\Sigma}^{\text{PS}}$, $\hat{A}_i^{(d)}$ and $\hat{B}_i^{(d)}$ deviate from their true versions by $\varepsilon^{\text{PS}}(\hat{A}_i^{(d)})$ and $\varepsilon^{\text{PS}}(\hat{B}_i^{(d)})$, bounded by:

$$\varepsilon^{\text{PS}}(\hat{A}_i^{(d)}) \leq 2\sqrt{\hat{A}_i^{(d)}} \Delta_{i,\mu} \sqrt{\frac{\lambda_{\max}(\hat{\Sigma}_i^{(d)})}{\tilde{\lambda}_{\min}(\hat{\Sigma}_i^{(d)})}} + \hat{A}_i^{(d)} \frac{\Delta_{i,\Sigma}}{\lambda_{\max}(\hat{\Sigma}_i^{(d)})}, \quad (101)$$

$$\varepsilon^{\text{PS}}(\hat{B}_i^{(d)}) \leq 2\sqrt{\hat{B}_i^{(d)}} \Delta_{j^*,\mu} \sqrt{\frac{\lambda_{\max}(\hat{\Sigma}_{j^*}^{(d)})}{\tilde{\lambda}_{\min}(\hat{\Sigma}_{j^*}^{(d)})}} + \hat{B}_i^{(d)} \frac{\Delta_{j^*,\Sigma}}{\lambda_{\max}(\hat{\Sigma}_{j^*}^{(d)})}, \quad (102)$$

where j^* is defined in (88). We avoid extremely loose bounds by replacing tiny, rarely observable eigenvalues, by a robust floor eigenvalue. Given a matrix $\mathbf{A} \in \mathbb{R}^{d \times d}$, we define $\tilde{\lambda}_{\min}(\mathbf{A})$ as (Horn & Johnson, 2013, Thm. 4.3.1):

$$\tilde{\lambda}_{\min}(\mathbf{A}) = \lambda_{\min}(\mathbf{A} + \epsilon_r \lambda_{\max}(\mathbf{A}) I^{(d)}), \quad (103)$$

where $\epsilon_r = 0.05$ is typically taken and $I^{(d)}$ is the identity matrix. Ultimately, let us define the Euclidean Lipschitz constant $L_{i,\text{lip}}$ as:

$$L_i^{\text{PS}} = \sqrt{\left(\frac{\partial \text{PS}_i}{\partial A_i}(A_i^{(d)}, B_i^{(d)}) \right)^2 + \left(\frac{\partial \text{PS}_i}{\partial B_i}(A_i^{(d)}, B_i^{(d)}) \right)^2} = \frac{\sqrt{(\hat{A}_i^{(d)})^2 + (\hat{B}_i^{(d)})^2}}{(\hat{A}_i^{(d)} + \hat{B}_i^{(d)})^2}, \quad (104)$$

which enables us to bound the finite-sample deviation of $\widehat{\text{PS}}_i^{(d)}$ with:

$$\left| \widehat{\text{PS}}_i^{(d)} - \text{PS}_i^{(d)} \right| \leq L_i^{\text{PS}} \sqrt{\varepsilon^{\text{PS}}(\hat{A}_i^{(d)}) + \varepsilon^{\text{PS}}(\hat{B}_i^{(d)})}. \quad (105)$$

Finally, we employ the triangle inequality on both error sources (95) and (105) and obtain for $\delta_i^{\text{PS}} = \delta_{i,\mu}^{\text{PS}} + \delta_{i,\Sigma}^{\text{PS}}$, with $\delta_i^{\text{PS}} \in (0, 1)$:

$$\mathbb{P}_{\pi} \left\{ \left| \widehat{\text{PS}}_i^{(d)} - \text{PS}_i \right| \leq \frac{\hat{B}_i^{(d)} \sqrt{\mathbf{r}_{i,i}^T \mathbf{S}_i^{-1} \mathbf{r}_{i,i}} + \hat{A}_i^{(d)} \sqrt{\mathbf{r}_{i,j^*}^T \mathbf{S}_{j^*}^{-1} \mathbf{r}_{i,j^*}}}{\left(\hat{A}_i^{(d)} + \hat{B}_i^{(d)} \right)^2} + L_i^{\text{PS}} \sqrt{\varepsilon^{\text{PS}} \left(\hat{A}_i^{(d)} \right) + \varepsilon^{\text{PS}} \left(\hat{B}_i^{(d)} \right)} \right\} \geq 1 - \delta_i^{\text{PS}}. \quad (106)$$

We now analyze the obtained expression separately for the deterministic and probabilistic terms. In the former term, the two square-root terms are energies that leak into the truncated complement after regressing out the retained d diffusion coordinates. Intuitively, $\Sigma_j^{(d)}$ encodes the local anisotropy of cluster j in the kept coordinates, C_j represents coupling of residual energy in the truncated block, and $\Sigma_j^{(\perp)}$ is the spread that remains in the truncated block. Therefore, larger S_j down-weights complement deviations, reducing the bias, while $\mathbf{r}_{i,j}$ and S_j co-vary through the cross-covariance C_j . Namely, increasing C_j shrinks both $\mathbf{r}_{i,j}$ and S_j , while decreasing C_j does the opposite. The practical rule is to prevent tiny $\lambda_{\min}(S_j)$, e.g., by promoting such directions into the kept set via a local choice of d , and shape distortions so the complement is predictable from the kept coordinates, keeping $\mathbf{r}_{i,j}$ small.

For the probabilistic part, its width reflects uncertainty in the empirical centroid and covariance of the attributed and nearest foreign clusters, where $\lambda_{\max}(\widehat{\Sigma}_j^{(d)})$ and $n_{j,\text{eff}}$ determine the width primarily. Practically, correlated distortions shrink $n_{j,\text{eff}}$ and widen the bound, and a smaller spectral flatness ratio r_j yields tighter matrix concentration. As expected, the probabilistic piece dominates the deterministic as shown in Figure 9, which underlines the importance of cluster construction and dependence control.

B.2 THE PM MEASURE

As in the PS case, we start with the truncation error and assume access to cluster statistics. Let us reconsider Eqs. (70)–(82), but with two adjustments. First, the cluster coordinates are centered around the cluster reference embedding and not the cluster mean. Given $m = N - d - 1$, we define:

$$\Delta_{i,p}^{(d)} = \Psi_t^{(d)}(\mathbf{x}_{i,p}) - \Psi_t^{(d)}(\mathbf{x}_{i,0}) \in \mathbb{R}^d, \quad (107)$$

$$\Delta_{i,p}^{(\perp)} = \Psi_t^{(\perp)}(\mathbf{x}_{i,p}) - \Psi_t^{(\perp)}(\mathbf{x}_{i,0}) \in \mathbb{R}^m. \quad (108)$$

Second, the cluster is now absent the reference embedding. Namely, the full $N - 1$ -dimensional cluster is (75):

$$\tilde{c}_i = c_i \setminus \Psi_t(\mathbf{x}_i). \quad (109)$$

The cluster \tilde{c}_i has difference $\Delta_{i,p} \in \mathbb{R}^{N-1}$ for every $p \in \{1, \dots, N_p\}$ and covariance $\tilde{\Sigma}_i \in \mathbb{R}^{(N-1) \times (N-1)}$ that hold (28):

$$\Delta_{i,p} = \begin{bmatrix} \Delta_{i,p}^{(d)} \\ \Delta_{i,p}^{(\perp)} \end{bmatrix}, \quad \tilde{\Sigma}_i = \begin{bmatrix} \tilde{\Sigma}_i^{(d)} & \tilde{C}_i \\ \tilde{C}_i^T & \tilde{\Sigma}_i^{(\perp)} \end{bmatrix}, \quad (110)$$

with $\tilde{\Sigma}_i^{(\perp)} \in \mathbb{R}^{m \times m}$ and $\tilde{C}_i \in \mathbb{R}^{d \times m}$ being:

$$\tilde{\Sigma}_i^{(\perp)} = \frac{1}{|\tilde{c}_i^{(\perp)}| - 1} \sum_{\psi \in \tilde{c}_i^{(\perp)}} \left(\psi - \Psi_t^{(\perp)}(\mathbf{x}_i) \right) \left(\psi - \Psi_t^{(\perp)}(\mathbf{x}_i) \right)^T, \quad (111)$$

$$\tilde{C}_i = \frac{1}{|\tilde{c}_i^{(\perp)}| - 1} \sum_{p=1}^{N_p} \left(\Psi_t^{(d)}(\mathbf{x}_{i,p}) - \Psi_t^{(d)}(\mathbf{x}_i) \right) \left(\Psi_t^{(\perp)}(\mathbf{x}_{i,p}) - \Psi_t^{(\perp)}(\mathbf{x}_i) \right)^T. \quad (112)$$

In $N - 1$ dimensions, the squared Mahalanobis distance from $\Psi_t(\mathbf{x}_{i,p})$ to \tilde{c}_i is given by (24):

$$d_M^2 \left(\Psi_t(\mathbf{x}_{i,p}); \Psi_t(\mathbf{x}_{i,0}), \tilde{\Sigma}_i \right) = \Delta_{i,p}^T \left(\tilde{\Sigma}_i + \epsilon I^{(N-1)} \right)^{-1} \Delta_{i,p}, \quad (113)$$

where as in (79), inversion has been empirically obtained with $\epsilon = 10^{-6}$ and the $N - 1$ -dimensional identity matrix $I^{(N-1)}$. We again turn to the Schur complement Horn & Johnson (2013) and decompose (113):

$$d_M^2 \left(\Psi_t(\mathbf{x}_{i,p}); \Psi_t(\mathbf{x}_{i,0}), \tilde{\Sigma}_i \right) = \left(\Delta_{i,p}^{(d)} \right)^T \left(\tilde{\Sigma}_i^{(d)} + \epsilon I^{(d)} \right)^{-1} \Delta_{i,p}^{(d)} + \mathbf{r}_{i,p}^T \mathbf{S}_i^{-1} \mathbf{r}_{i,p}, \quad (114)$$

with $\mathbf{r}_{i,p} \in \mathbb{R}^m$ and the Schur complement $\mathbf{S}_i \in \mathbb{R}^{m \times m}$ being:

$$\mathbf{r}_{i,p} = \Delta_{i,p}^{(\perp)} - \tilde{\mathbf{C}}_i^T \left(\tilde{\Sigma}_i^{(d)} + \epsilon I^{(d)} \right)^{-1} \Delta_{i,p}^{(d)}, \quad (115)$$

$$\mathbf{S}_i = \tilde{\Sigma}_i^{(\perp)} - \tilde{\mathbf{C}}_i^T \left(\tilde{\Sigma}_i^{(d)} + \epsilon I^{(d)} \right)^{-1} \tilde{\mathbf{C}}_i. \quad (116)$$

Let us define the set of squared Mahalanobis distances of cluster \tilde{c}_i in dimension $N - 1$ as:

$$\mathcal{G}_i = \left\{ d_M^2 \left(\Psi_t(\mathbf{x}_{i,p}); \Psi_t(\mathbf{x}_i), \tilde{\Sigma}_i \right) \mid p = 1, \dots, N_p \right\}, \quad (117)$$

in accordance to the truncated version of $\mathcal{G}_i^{(d)}$ in (30). By employing (114), for every $p \in \{1, \dots, N_p\}$, we can bound the truncation error of the squared Mahalanobis distance as follows:

$$d_M^2 \left(\Psi_t(\mathbf{x}_{i,p}); \Psi_t(\mathbf{x}_{i,0}), \tilde{\Sigma}_i \right) - d_M^2 \left(\Psi_t^{(d)}(\mathbf{x}_{i,p}); \Psi_t^{(d)}(\mathbf{x}_{i,0}), \tilde{\Sigma}_i^{(d)} \right) = \mathbf{r}_{i,p}^T \mathbf{S}_i^{-1} \mathbf{r}_{i,p} := \delta_{\mathcal{G}_i,p}, \quad (118)$$

and the difference between the mean of the elements in \mathcal{G}_i and $\mathcal{G}_i^{(d)}$ can be expressed as:

$$\begin{aligned} \mu_{\mathcal{G}_i} - \mu_{\mathcal{G}_i^{(d)}} &= \frac{1}{|\mathcal{G}_i|} \sum_{g \in \mathcal{G}_i} g - \frac{1}{|\mathcal{G}_i^{(d)}|} \sum_{g \in \mathcal{G}_i^{(d)}} g = \frac{1}{N_p} \sum_{p=1}^{N_p} \mathbf{r}_{i,p}^T \mathbf{S}_i^{-1} \mathbf{r}_{i,p} = \\ &= \frac{1}{N_p} \sum_{p=1}^{N_p} \delta_{\mathcal{G}_i,p} := \delta_{\mathcal{G}_i,\mu}. \end{aligned} \quad (119)$$

Similarly, we can express the deviation of the variance:

$$\sigma_{\mathcal{G}_i}^2 - \sigma_{\mathcal{G}_i^{(d)}}^2 = \frac{1}{|\mathcal{G}_i| - 1} \sum_{g \in \mathcal{G}_i} (g - \mu_{\mathcal{G}_i})^2 - \frac{1}{|\mathcal{G}_i^{(d)}| - 1} \sum_{g \in \mathcal{G}_i^{(d)}} (g - \mu_{\mathcal{G}_i^{(d)}})^2, \quad (120)$$

and with (119) and the Cauchy-Schwartz inequality, we can obtain:

$$\left| \sigma_{\mathcal{G}_i}^2 - \sigma_{\mathcal{G}_i^{(d)}}^2 \right| \leq \frac{N_p}{N_p - 1} \left(2\delta_{\mathcal{G}_i,p}^{\max} \left(\sigma_{\mathcal{G}_i} + \sigma_{\mathcal{G}_i^{(d)}} \right) + (\delta_{\mathcal{G}_i,p}^{\max})^2 \right), \quad (121)$$

where $\delta_{\mathcal{G}_i,p}^{\max} = \max_p \delta_{\mathcal{G}_i,p}$. The Gamma-matching parameters in the truncated and full dimensions are (33):

$$k_i^{(d)} = \frac{\mu_{\mathcal{G}_i^{(d)}}^2}{\sigma_{\mathcal{G}_i^{(d)}}^2}, \quad k_i = \frac{\mu_{\mathcal{G}_i}^2}{\sigma_{\mathcal{G}_i}^2}, \quad (122)$$

$$\theta_i^{(d)} = \frac{\sigma_{\mathcal{G}_i^{(d)}}^2}{\mu_{\mathcal{G}_i^{(d)}}}, \quad \theta_i = \frac{\sigma_{\mathcal{G}_i}^2}{\mu_{\mathcal{G}_i}}, \quad (123)$$

and their deviations can be bounded by considering (119), (121):

$$\left| k_i - k_i^{(d)} \right| \leq C_1 \delta_{\mathcal{G}_i,p}^{\max} \frac{N_p}{N_p - 1} \frac{\mu_{\mathcal{G}_i} + \mu_{\mathcal{G}_i^{(d)}}}{\sigma_{\mathcal{G}_i^{(d)}}^2} := \delta_{\mathcal{G}_i,k}, \quad (124)$$

$$\left| \theta_i - \theta_i^{(d)} \right| \leq C_2 \delta_{\mathcal{G}_i,p}^{\max} \frac{N_p}{N_p - 1} \frac{\sigma_{\mathcal{G}_i}^2 + \sigma_{\mathcal{G}_i^{(d)}}^2}{\mu_{\mathcal{G}_i^{(d)}}^2} := \delta_{\mathcal{G}_i,\theta}, \quad (125)$$

with universal constants $C_1, C_2 > 0$. Recalling (35), let the squared Mahalanobis distance from the output embedding to the cluster be:

$$d_M^2 \left(\Psi_t^{(d)}(\hat{\mathbf{x}}_i); \Psi_t^{(d)}(\mathbf{x}_i), \tilde{\Sigma}_i^{(d)} \right) := a_i, \quad (126)$$

and employing (118) for the output embedding yields:

$$d_M^2 \left(\Psi_t(\hat{\mathbf{x}}_i); \Psi_t(\mathbf{x}_{i,0}), \tilde{\Sigma}_i \right) - d_M^2 \left(\Psi_t^{(d)}(\hat{\mathbf{x}}_i); \Psi_t^{(d)}(\mathbf{x}_{i,0}), \tilde{\Sigma}_i^{(d)} \right) = \mathbf{r}_{i,a}^T \mathbf{S}_i^{-1} \mathbf{r}_{i,a} := \delta_{\mathcal{G}_i,a}. \quad (127)$$

As in (36), the PM definition in dimension $N - 1$ can be expressed using the regularized upper incomplete gamma function $Q(k, x) = \Gamma(k, x)/\Gamma(k)$:

$$\text{PM}_i = Q \left(k_i, \frac{a_i}{\theta_i} \right). \quad (128)$$

Consider the truncation-induced ellipsoid:

$$\mathcal{B}_i = \left\{ (k'_i, \theta'_i, a'_i) : \left| k'_i - k_i^{(d)} \right| \leq \delta_{\mathcal{G}_i,k}, \left| \theta'_i - \theta_i^{(d)} \right| \leq \delta_{\mathcal{G}_i,\theta}, \left| a'_i - a_i^{(d)} \right| \leq \delta_{\mathcal{G}_i,a} \right\}, \quad (129)$$

For $F(k, \theta, a) = Q(k, a/\theta)$, the gradient with the partial derivatives with respect to k, θ and a is:

$$\nabla F(k, \theta, a) = \begin{pmatrix} \frac{1}{\Gamma(k)} \int_x^\infty t^{k-1} e^{-t} \ln t \, dt - \psi(k) Q(k, x) \\ \frac{a}{\theta^2} \frac{x^{k-1} e^{-x}}{\Gamma(k)} \\ -\frac{1}{\theta} \frac{x^{k-1} e^{-x}}{\Gamma(k)} \end{pmatrix}, \quad (130)$$

where $x = a/\theta$ and $\psi(\cdot)$ is the digamma function. Since $\nabla F(k, \theta, a)$ is continuous and bounded on the compact set \mathcal{B}_i , we set:

$$L_{\mathcal{B}_i} = \sup_{(k, \theta, a) \in \mathcal{B}_i} \|\nabla F(k, \theta, a)\|_2 < \infty. \quad (131)$$

To yield the bound on the PM measure due to truncation, we notice that both (k_i, θ_i, a_i) and $(k_i^{(d)}, \theta_i^{(d)}, a_i^{(d)})$ lie in \mathcal{B}_i , and apply the multivariate mean-value theorem to yield the following:

$$\left| \text{PM}_i - \text{PM}_i^{(d)} \right| \leq L_{\mathcal{B}_i} \left(\delta_{\mathcal{G}_i,k}^2 + \delta_{\mathcal{G}_i,\theta}^2 + \delta_{\mathcal{G}_i,a}^2 \right)^{1/2}. \quad (132)$$

However, this bound can be tightened. We notice that $Q(k, x)$ (36) is monotonically increasing in k and decreasing in x , for $k, x > 0$ (130). We assume that on \mathcal{B}_i , and for all $(\theta, a) \in \mathcal{B}_i$, $\partial F/\partial k$ does not change signs, or otherwise we fallback to (132). Consequently, the maximal change of $Q(k, x)$ inside \mathcal{B}_i is attained at one of its eight corners, and (132) can be tightened to this PM error radius:

$$\left| \text{PM}_i - \text{PM}_i^{(d)} \right| \leq \max_{(k_c, \theta_c, a_c) \in \partial \mathcal{B}_i} \left| Q(k_c, a_c/\theta_c) - Q(\hat{k}_i^{(d)}, \hat{a}_i^{(d)}/\hat{\theta}_i^{(d)}) \right|. \quad (133)$$

As in the PS case, we now analyze how the finite number of coordinates in a cluster leads to uncertainty in the PM evaluation. Let R_i be the maximal squared Mahalanobis distance in \mathcal{G}_i , namely:

$$R_i = \max_{g \in \mathcal{G}_i} g. \quad (134)$$

Again, similarly to the PS case, we utilize the vector and matrix Bernstein (Vershynin, 2024, Props. 2.8.1, 4.7.1) and the dependent Hanson-Wright inequalities (Adamczak, 2015, Thm. 2.5). Let us consider the confidence parameters $\delta_{i,\mu}^{\text{PM}}, \delta_{i,\sigma}^{\text{PM}}, \delta_{i,a}^{\text{PM}} \in (0, 1/3)$, so with respective least probabilities of $1 - \delta_{i,\mu}^{\text{PM}}, 1 - \delta_{i,\sigma}^{\text{PM}}, 1 - \delta_{i,a}^{\text{PM}}$:

$$\left| \mu_{\mathcal{G}_i^{(d)}} - \hat{\mu}_{\mathcal{G}_i^{(d)}} \right| \leq \sqrt{\frac{2\hat{\sigma}_{\mathcal{G}_i^{(d)}}^2 \ln(2/\delta_{i,\mu}^{\text{PM}})}{N_p}} + \frac{3R_i \ln(2/\delta_{i,\mu}^{\text{PM}})}{N_p} := \Delta_{i,\mu}, \quad (135)$$

$$\left| \sigma_{\mathcal{G}_i^{(d)}} - \hat{\sigma}_{\mathcal{G}_i^{(d)}} \right| \leq \sqrt{\frac{2R_i^2 \ln(2/\delta_{i,\sigma}^{\text{PM}})}{N_p}} + \frac{3R_i^2 \ln(2/\delta_{i,\sigma}^{\text{PM}})}{N_p} := \Delta_{i,\sigma}, \quad (136)$$

$$\left| a_i - \hat{a}_i \right| \leq R_i \sqrt{\frac{\ln(2/\delta_{i,a}^{\text{PM}})}{N_p}} := \Delta_{i,a}. \quad (137)$$

Recalling the definition of $k_i^{(d)}$, $\theta_i^{(d)}$ from (122), (123), since by design $\hat{\mu}_{\mathcal{G}_i^{(d)}} > 0$, and since we empirically validate that $\Delta_{i,\mu} \ll \hat{\mu}_{\mathcal{G}_i^{(d)}}$, $\Delta_{i,\sigma} \ll \hat{\sigma}_{\mathcal{G}_i^{(d)}}$, we can apply the first-order Taylor expansions to $k_i^{(d)}$, $\theta_i^{(d)}$ around $\hat{k}_i^{(d)}$, $\hat{\theta}_i^{(d)}$, respectively. Apply the triangle inequality to it gives:

$$\left| k_i^{(d)} - \hat{k}_i^{(d)} \right| \leq \left| \frac{\partial k_i^{(d)}}{\partial \mu} \right| \Delta_{i,\mu} + \left| \frac{\partial k_i^{(d)}}{\partial \sigma} \right| \Delta_{i,\sigma} = \left| \frac{2\hat{\mu}_{\mathcal{G}_i^{(d)}}}{\hat{\sigma}_{\mathcal{G}_i^{(d)}}^2} \right| \Delta_{i,\mu} + \left| \frac{-2\hat{\mu}_{\mathcal{G}_i^{(d)}}^2}{\hat{\sigma}_{\mathcal{G}_i^{(d)}}^3} \right| \Delta_{i,\sigma} := \Delta_{i,k}, \quad (138)$$

$$\left| \theta_i^{(d)} - \hat{\theta}_i^{(d)} \right| \leq \left| \frac{\partial \theta_i^{(d)}}{\partial \mu} \right| \Delta_{i,\mu} + \left| \frac{\partial \theta_i^{(d)}}{\partial \sigma} \right| \Delta_{i,\sigma} = \left| \frac{-\hat{\sigma}_{\mathcal{G}_i^{(d)}}^2}{\hat{\mu}_{\mathcal{G}_i^{(d)}}^2} \right| \Delta_{i,\mu} + \left| \frac{2\hat{\sigma}_{\mathcal{G}_i^{(d)}}}{\hat{\mu}_{\mathcal{G}_i^{(d)}}} \right| \Delta_{i,\sigma} := \Delta_{i,\theta}. \quad (139)$$

Empirically, rarely $\Delta_{i,k}$, $\Delta_{i,\theta}$ or $\Delta_{i,a}$ become extremely loose. To avoid this behavior, we practically regularize the box by setting:

$$\Delta_{i,k} \rightarrow \min \left(\Delta_{i,k}, 0.5k_i^{(d)} \right), \quad (140)$$

$$\Delta_{i,\theta} \rightarrow \min \left(\Delta_{i,\theta}, 0.5\theta_i^{(d)} \right), \quad (141)$$

$$\Delta_{i,a} \rightarrow \min \left(\Delta_{i,a}, 0.5a_i^{(d)} \right). \quad (142)$$

Let us consider the local box of values:

$$\mathcal{B}_i^{\text{loc}} = \left\{ (k'_i, \theta'_i, a'_i) : k'_i \in [k_i^{(d)} \pm \Delta_{i,k}], \theta'_i \in [\theta_i^{(d)} \pm \Delta_{i,\theta}], a'_i \in [a_i^{(d)} \pm \Delta_{i,a}] \right\}. \quad (143)$$

As discussed earlier, $Q(k, x)$ is monotonically increasing in k and decreasing in x , for $k, x > 0$ (130). Consequently, the maximal change of $Q(k, x)$ inside $\mathcal{B}_i^{\text{loc}}$ is attained at one of its eight corners. Thus, the finite-sample error of the PM measure in dimension d is bounded by:

$$\left| \text{PM}_i^{(d)} - \widehat{\text{PM}}_i^{(d)} \right| \leq \max_{(k_c, \theta_c, a_c) \in \partial \mathcal{B}_i^{\text{loc}}} \left| Q(k_c, a_c/\theta_c) - Q(\hat{k}_i^{(d)}, \hat{a}_i^{(d)}/\hat{\theta}_i^{(d)}) \right|. \quad (144)$$

Ultimately, we combine the deterministic error radius with the probabilistic width. Let $\delta_i^{\text{PM}} = \delta_{i,\mu}^{\text{PM}} + \delta_{i,\sigma}^{\text{PM}} + \delta_{i,a}^{\text{PM}}$, which yields for $\delta_i^{\text{PM}} \in (0, 1)$:

$$\begin{aligned} \mathbb{P}_{\boldsymbol{\pi}} \left\{ \left| \widehat{\text{PM}}_i^{(d)} - \text{PM}_i \right| \leq \right. \\ \left. \max_{(k_c, \theta_c, a_c) \in \partial \mathcal{B}_i} \left| Q(k_c, a_c/\theta_c) - Q(\hat{k}_i^{(d)}, \hat{a}_i^{(d)}/\hat{\theta}_i^{(d)}) \right| + \right. \\ \left. \max_{(k_c, \theta_c, a_c) \in \partial \mathcal{B}_i^{\text{loc}}} \left| Q(k_c, a_c/\theta_c) - Q(\hat{k}_i^{(d)}, \hat{a}_i^{(d)}/\hat{\theta}_i^{(d)}) \right| \right\} \geq 1 - \delta_i^{\text{PM}}. \end{aligned} \quad (145)$$

In the deterministic term, large cross-block coupling $\tilde{\mathbf{C}}_i$ or residual spread $\tilde{\boldsymbol{\Sigma}}_i^{(\perp)}$ again directly inflate the error radius via the Schur complement.

In the probabilistic part, the local box $\mathcal{B}_i^{\text{loc}}$ aggregates two finite-sample pieces. The first is the uncertainty of the moment, with $\Delta_{i,\mu}$ and $\Delta_{i,\sigma}$ scale as $1/N_p$ but are amplified by the maximal radius of Mahalanobis within the cluster R_i . Heavy outliers increase R_i and widen both bounds. The second is the uncertainty of the distance of the output, contributed by $\Delta_{i,a}$ which is also proportional to R_i but scales by $1/\sqrt{N_p}$. Again, this emphasizes the importance of the design of distortions.

C ERROR RADIUS AND PROBABILISTIC CONFIDENCE BOUND OF THE PCC AND SRCC

In this Appendix, we propagate the frame-level error radius and probabilistic widths developed in Appendix B.1 and B.2 to the reported PCC and SRCC values. e.g., as reported in Table 4.

We start by fixing a trial l , a source separation system q , and a time frame f . Let the indices of the active sources in frame f be \mathcal{S}_f^l and consider a source $i \in \mathcal{S}_f^l$. The observation of measure $\mathcal{P} \in \{\text{PS}, \text{PM}\}$, denoted $\hat{v}_{i,f}^{q,l,\mathcal{P}}$, can be decomposed as:

$$\hat{v}_{i,f}^{q,l,\mathcal{P}} = v_{i,f}^{q,l,\mathcal{P}} + \tilde{\beta}_{i,f}^{q,l,\mathcal{P}} + \zeta_{i,f}^{q,l,\mathcal{P}}, \quad (146)$$

where:

$$\tilde{\beta}_{i,f}^{q,l,\mathcal{P}} = \beta_{i,f}^{q,l,\mathcal{P}} + \mu_{i,f}^{q,l,\mathcal{P}}, \quad (147)$$

and $\beta_{i,f}^{q,l,\mathcal{P}}$ is an unknown deterministic bias with a provided radius $b_{i,f}^{q,l,\mathcal{P}}$, such that:

$$|\beta_{i,f}^{q,l,\mathcal{P}}| \leq b_{i,f}^{q,l,\mathcal{P}}, \quad (148)$$

with $b_{i,f}^{q,l,\mathcal{P}}$ given by either (95) or (133). Regarding the probabilistic side, we define:

$$\zeta_{i,f}^{q,l,\mathcal{P}} = \varepsilon_{i,f}^{q,l,\mathcal{P}} - \mu_{i,f}^{q,l,\mathcal{P}}, \quad (149)$$

where:

$$\varepsilon_{i,f}^{q,l,\mathcal{P}} = \hat{v}_{i,f}^{q,l,\mathcal{P}} - v_{i,f}^{q,l,\mathcal{P}}, \quad (150)$$

and $\mathbb{E}_{\pi}(\zeta_{i,f}^{q,l,\mathcal{P}}) = 0$. Thus, the two-sided probabilistic half-width $p_{i,f}^{q,l,\mathcal{P}} \geq 0$ can be interpreted as:

$$\mathbb{P}_{\pi} \left(|\varepsilon_{i,f}^{q,l,\mathcal{P}} - \mu_{i,f}^{q,l,\mathcal{P}}| \leq p_{i,f}^{q,l,\mathcal{P}} \right) \geq 1 - \delta^{\mathcal{P}} := c^{\mathcal{P}}, \quad (151)$$

with $\delta^{\mathcal{P}}$ and the probabilistic bounds defined in (105) and (144). We abbreviate $c^{\mathcal{P}}$ as c from now on. Consider z_{c^*} the normal quantile at level $c^* = (1 + c)/2$, so we calibrate the half-widths scale to be:

$$\sigma_{i,f}^{q,l,\mathcal{P}} = \frac{c}{z_{c^*}}, \quad (152)$$

with tails still reported back as half-widths at the original confidence c .

We now propagate these errors from frame to utterance level, based on the aggregations we introduced in (37) and (41). On average, experiments showed that frames more than $g = 4$ apart are effectively independent both for speech and music mixtures. Given the set \mathcal{F}^l of time frames with two or more active sources, the standard Bartlett block-decimation Bartlett (1946) yields the conservative inflation:

$$\text{std} \left(\frac{1}{\mathcal{F}^l} \sum_{f=1}^{\mathcal{F}^l} \zeta_{i,f}^{q,l,\mathcal{P}} \right) \leq \frac{\sqrt{g+1}}{\sqrt{\mathcal{F}^l}} \left(\frac{1}{\mathcal{F}^l} \sum_{f=1}^{\mathcal{F}^l} \left(\sigma_{i,f}^{q,l,\mathcal{P}} \right)^2 \right)^{1/2}. \quad (153)$$

Let the radius error and the p -level probabilistic half-width obtained at the utterance-level using average pooling equal, respectively:

$$b_{i,\text{average}}^{q,l,\mathcal{P}} = \frac{1}{\mathcal{F}^l} \sum_{f=1}^{\mathcal{F}^l} b_{i,f}^{q,l,\mathcal{P}}, \quad (154)$$

$$h_{i,\text{average}}^{q,l,\mathcal{P}} = z_{c^*} \frac{\sqrt{g+1}}{\sqrt{\mathcal{F}^l}} \left(\frac{1}{\mathcal{F}^l} \sum_{f=1}^{\mathcal{F}^l} \left(\sigma_{i,f}^{q,l,\mathcal{P}} \right)^2 \right)^{1/2}. \quad (155)$$

For the PESQ-like aggregation, let us denote its aggregation function from (41) as:

$$s(u) = 0.999 + 4(1 + \exp(-1.3669u + 3.8224))^{-1}. \quad (156)$$

Let W be the window and H the hop of frame used for aggregation, then M^l is the maximal number of possible windows. By norm submultiplicativity and the mean-value theorem (Horn & Johnson, 2013, Sec. 5.6):

$$b_{i,\text{pesq}}^{q,l,\mathcal{P}} = \frac{C_{\text{OL}}}{\sqrt{M^l}} \left(\frac{1}{\mathcal{F}^l} \sum_{f=1}^{\mathcal{F}^l} (b_f^{q,l,\mathcal{P}})^2 \right)^{1/2} \frac{\partial s}{\partial u}, \quad (157)$$

$$h_{i,\text{pesq}}^{q,l,\mathcal{P}} = z_{c^*} \frac{C_{\text{OL}}}{\sqrt{M^l}} \left(\frac{1}{\mathcal{F}^l} \sum_{f=1}^{\mathcal{F}^l} (\sigma_f^{q,l,\mathcal{P}})^2 \right)^{1/2} \frac{\partial s}{\partial u}, \quad (158)$$

where $C_{\text{OL}} = \lceil W/H \rceil$ and by construction $\partial s / \partial u \leq 1.3669$ when evaluated at point u .

To translate utterance-level errors to source-based PCC and SRCC values, let the integration of utterance-level MOS ratings from every system $q \in \{1, \dots, Q\}$ be:

$$\mathbf{v}_{i,\text{MOS}}^l = (v_{i,\text{MOS}}^{1,l}, \dots, v_{i,\text{MOS}}^{Q,l}), \quad (159)$$

and similarly, denoting $\hat{v}_{i,\mathcal{A}}^{q,l,\mathcal{P}}$ as the estimated aggregated measure across systems, where \mathcal{A} is either average or PESQ-like aggregation (4.2), then its integration is given by:

$$\hat{\mathbf{v}}_{i,\mathcal{A}}^{l,\mathcal{P}} = (\hat{v}_{i,\mathcal{A}}^{1,l,\mathcal{P}}, \dots, \hat{v}_{i,\mathcal{A}}^{Q,l,\mathcal{P}}). \quad (160)$$

For every vector \mathbf{v} , we denote its centered version by $\tilde{\mathbf{v}}$. Let us denote the PCC value between an observation vector \mathbf{v} and a MOS vector \mathbf{m} as $r^{\text{PCC}}(\mathbf{v}, \mathbf{m})$, according to (45) and (46). Its gradient with respect to \mathbf{v} at point $\hat{\mathbf{v}}_{i,\mathcal{A}}^{l,\mathcal{P}}$ is Benesty et al. (2009):

$$\left. \frac{\partial r^{\text{PCC}}}{\partial \mathbf{v}} \right|_{\mathbf{v}=\hat{\mathbf{v}}_{i,\mathcal{A}}^{l,\mathcal{P}}} = \frac{\mathbf{v}_{i,\text{MOS}}^l}{\|\hat{\mathbf{v}}_{i,\mathcal{A}}^{l,\mathcal{P}}\|_2 \|\mathbf{v}_{i,\text{MOS}}^l\|_2} - \frac{r^{\text{PCC}}(\hat{\mathbf{v}}_{i,\mathcal{A}}^{l,\mathcal{P}}, \mathbf{v}_{i,\text{MOS}}^l)}{\|\hat{\mathbf{v}}_{i,\mathcal{A}}^{l,\mathcal{P}}\|_2^2} \hat{\mathbf{v}}_{i,\mathcal{A}}^{l,\mathcal{P}}. \quad (161)$$

Consider $\mathbf{b}_{i,\mathcal{A}}^{l,\mathcal{P}}$ the utterance-level bias radii from (154) or (157) across all systems:

$$\mathbf{b}_{i,\mathcal{A}}^{l,\mathcal{P}} = (b_{i,\mathcal{A}}^{1,l,\mathcal{P}}, \dots, b_{i,\mathcal{A}}^{Q,l,\mathcal{P}}). \quad (162)$$

Then, the induced PCC bias can be bounded by:

$$b_{i,\mathcal{A}}^{l,\mathcal{P},\text{PCC}} \leq \left\| \frac{\partial r^{\text{PCC}}}{\partial \hat{\mathbf{v}}_{i,\mathcal{A}}^{l,\mathcal{P}}} \right\|_2 \|\tilde{\mathbf{b}}_{i,\mathcal{A}}^{l,\mathcal{P}}\|_2. \quad (163)$$

For the probabilistic half-width, we model independent Gaussian jitters across systems with scales fixed by the utterance half-widths. Consider the Q -dimensional Gaussian vector:

$$\boldsymbol{\eta} \sim \mathcal{N}\left(\mathbf{0}, \text{diag}\left(\left(\frac{h_{i,\mathcal{A}}^{1,l,\mathcal{P}}}{z_{c^*}}\right)^2, \dots, \left(\frac{h_{i,\mathcal{A}}^{Q,l,\mathcal{P}}}{z_{c^*}}\right)^2\right)\right), \quad (164)$$

with $\mathbf{0} \in \mathbb{R}^Q$. Using the delta method, first-order error propagation gives:

$$h_{i,\mathcal{A}}^{l,\mathcal{P},\text{PCC}} = z_{c^*} \sqrt{\left(\frac{\partial r^{\text{PCC}}}{\partial \hat{\mathbf{v}}_{i,\mathcal{A}}^{l,\mathcal{P}}} \right)^T \text{diag}\left(\left(\frac{h_{i,\mathcal{A}}^{1,l,\mathcal{P}}}{z_{c^*}}\right)^2, \dots, \left(\frac{h_{i,\mathcal{A}}^{Q,l,\mathcal{P}}}{z_{c^*}}\right)^2\right) \left(\frac{\partial r^{\text{PCC}}}{\partial \hat{\mathbf{v}}_{i,\mathcal{A}}^{l,\mathcal{P}}} \right)}. \quad (165)$$

Turning to the SRCC, let $\rho^{\text{SRCC}}(\cdot, \cdot)$ denote Spearman's rank correlation between two vectors Kendall & Gibbons (1990), as defined in (47) and (48). Because ranks are piecewise-constant, a safe deterministic error radius is obtained by checking the two extreme bias orientations:

$$b_{i,\mathcal{A}}^{l,\mathcal{P},\text{SRCC}} = \max\left(\left| \rho^{\text{SRCC}}(\hat{\mathbf{v}}_{i,\mathcal{A}}^{l,\mathcal{P}} + \mathbf{b}_{i,\mathcal{A}}^{l,\mathcal{P}}, \mathbf{v}_{i,\text{MOS}}^l) - \rho^{\text{SRCC}}(\hat{\mathbf{v}}_{i,\mathcal{A}}^{l,\mathcal{P}}, \mathbf{v}_{i,\text{MOS}}^l) \right|, \right. \\ \left. \left| \rho^{\text{SRCC}}(\hat{\mathbf{v}}_{i,\mathcal{A}}^{l,\mathcal{P}} - \mathbf{b}_{i,\mathcal{A}}^{l,\mathcal{P}}, \mathbf{v}_{i,\text{MOS}}^l) - \rho^{\text{SRCC}}(\hat{\mathbf{v}}_{i,\mathcal{A}}^{l,\mathcal{P}}, \mathbf{v}_{i,\text{MOS}}^l) \right| \right). \quad (166)$$

For the probabilistic half-width we jitter $\hat{\mathbf{v}}_{i,\mathcal{A}}^{l,\mathcal{P}}$ with the same independent Gaussian model in (164) and report the empirical c^* quantile from Monte Carlo of the following:

$$h_{i,\mathcal{A}}^{l,\mathcal{P},\text{SRCC}} = \text{Quantile}_{c^*} \left(\left| \rho^{\text{SRCC}}(\hat{\mathbf{v}}_{i,\mathcal{A}}^{l,\mathcal{P}} + \boldsymbol{\eta}, \mathbf{v}_{i,\text{MOS}}^l) - \rho^{\text{SRCC}}(\hat{\mathbf{v}}_{i,\mathcal{A}}^{l,\mathcal{P}}, \mathbf{v}_{i,\text{MOS}}^l) \right| \right), \quad (167)$$

where we used 10^4 draws for estimation, in the spirit of quantile bootstrap Efron & Tibshirani (1994).

Lastly, we consider the error propagation across all trials and their sources in a given scenario, e.g., English mixtures. Let \mathcal{L} denote the number of trials in a scenario, and for each trial $l \in \{1, \dots, \mathcal{L}\}$, assume the number of total speakers in the trial is N_{\max}^l (49). The values we report average across all \mathcal{L} trials and N_{\max}^l speakers, following (50)-(53).

The deterministic error radius of the PCC and SRCC per scenario are respectively given by:

$$b^{\text{PCC}} = \frac{1}{\sum_{l=1}^{\mathcal{L}} N_{\max}^l} \sum_{l=1}^{\mathcal{L}} \sum_{i=1}^{N_{\max}^l} b_{i,\mathcal{A}}^{l,\mathcal{P},\text{PCC}}, \quad (168)$$

$$b^{\text{SRCC}} = \frac{1}{\sum_{l=1}^{\mathcal{L}} N_{\max}^l} \sum_{l=1}^{\mathcal{L}} \sum_{i=1}^{N_{\max}^l} b_{i,\mathcal{A}}^{l,\mathcal{P},\text{SRCC}}. \quad (169)$$

To yield the probabilistic term, we assume that within any fixed trial l , the pairwise correlation between the source jitters has been empirically estimated and is denoted by ρ_l , while jitters from different trials are independent. This assumption holds by the construction of our trials in every scenario 4.1. Consequently, the c -level probabilistic half-width on the scenario mean equals:

$$h^{\text{PCC}} = \quad (170)$$

$$z_{c^*} \sqrt{\frac{1}{\left(\sum_{l=1}^{\mathcal{L}} N_{\max}^l\right)^2} \sum_{l=1}^{\mathcal{L}} \left(\sum_{i=1}^{N_{\max}^l} \left(\frac{h_{i,\mathcal{A}}^{l,\mathcal{P},\text{PCC}}}{z_{c^*}} \right)^2 + 2 \rho_l \sum_{\substack{i,j=1 \\ i < j}}^{N_{\max}^l} \left(\frac{h_{i,\mathcal{A}}^{l,\mathcal{P},\text{PCC}}}{z_{c^*}} \right) \left(\frac{h_{j,\mathcal{A}}^{l,\mathcal{P},\text{PCC}}}{z_{c^*}} \right) \right)}.$$

$$h^{\text{SRCC}} = \quad (171)$$

$$z_{c^*} \sqrt{\frac{1}{\left(\sum_{l=1}^{\mathcal{L}} N_{\max}^l\right)^2} \sum_{l=1}^{\mathcal{L}} \left(\sum_{i=1}^{N_{\max}^l} \left(\frac{h_{i,\mathcal{A}}^{l,\mathcal{P},\text{SRCC}}}{z_{c^*}} \right)^2 + 2 \rho_l \sum_{\substack{i,j=1 \\ i < j}}^{N_{\max}^l} \left(\frac{h_{i,\mathcal{A}}^{l,\mathcal{P},\text{SRCC}}}{z_{c^*}} \right) \left(\frac{h_{j,\mathcal{A}}^{l,\mathcal{P},\text{SRCC}}}{z_{c^*}} \right) \right)}.$$

Ultimately, for each scenario and each measure \mathcal{P} that uses aggregation technique \mathcal{A} , we report the deterministic envelope and probabilistic half-width b^{PCC} and h^{PCC} for PCC values and b^{SRCC} and h^{SRCC} for SRCC values.

D PERCEPTUAL DISTORTIONS AND THEIR PARAMETERS APPLIED TO THE PS AND PM

Table 6: Distortion bank used for the PM and PS measures. f_s is the sampling frequency, A_{95} marks the 95th-percentile absolute amplitude, and A_{RMS} the RMS amplitude of their respective signals.

Distortion	PS	PM
Notch Filter	Center frequencies: 500, 1000, 2000, 4000, 8000 Hz	Number of notches: ≤ 20 Operating band: 80 Hz - $0.45 f_s$ Notch spacing: ≥ 300 Hz Bandwidth: ± 60 Hz
Comb Filter	Delay: 2.5-15 ms Feedback gain: 0.4-0.9	Delay-gain pairs: (2.5 ms, 0.4), (5 ms, 0.5), (7.5 ms, 0.6), (10 ms, 0.7), (12.5 ms, 0.9)
Tremolo	Rate: 1, 2, 4, 6 Hz Depth: 0.3-1.0	Rate: 1, 2, 4, 6 Hz Depth: 1
Additive Noise	SNR: -15, -10, -5, 0, 5, 10, 15 dB Noise color: white, pink, brown	SNR: -15, -10, -5, 0, 5, 10, 15 dB Noise color: white, pink, brown
Additive Harmonic Tone	Tone frequency: 100, 500, 1000, 4000 Hz Amplitude: 0.02-0.08 (absolute)	Tone frequency: 100, 500, 1000, 4000 Hz Amplitude: $\{0.4, 0.6, 0.8, 1\} \times A_{\text{RMS}}$
Reverberation	RT_{60}: 0.3-1.1 s Early tail length: 5, 10, 15, 20 ms	Exponential tail length: 50, 100, 200, 400 ms Decay scaling: 0.3, 0.5, 0.7, 0.9
Noise Gate	Threshold: 0.005, 0.01, 0.02, 0.04 (absolute)	Threshold: $\{0.05, 0.1, 0.2, 0.4\} \times A_{95}$
Pitch Shift	Offsets: -4, -2, +2, +4 semitones	Offsets: -4, -2, +2, +4 semitones
Low-Pass Filter	Cutoff: 2000, 3000, 4000, 6000 Hz	Cutoff rule: spectral-energy quintiles: 50, 70, 85, 95% Rounding: nearest 100 Hz
High-Pass Filter	Cutoff: 100, 300, 500, 800 Hz	Cutoff rule: spectral-energy quintiles: 5, 15, 30, 50% Rounding: nearest 100 Hz
Echo	Delay: 5-20 ms Gain: 0.3-0.7	Delay: 50, 100, 150 ms Gain: 0.4, 0.5, 0.7
Hard Clipping	Threshold: 0.3, 0.5, 0.7 (absolute)	Threshold: $\{0.3, 0.5, 0.7\} \times A_{95}$
Vibrato	Rate: 3, 5, 7 Hz Depth: 0.001-0.003 (fractional stretch)	Rate: 3, 5, 7 Hz Depth: adaptive, clipped to 0.01-0.05

E TEMPORAL AND SPECTRAL EXAMPLES OF THE MEASURES

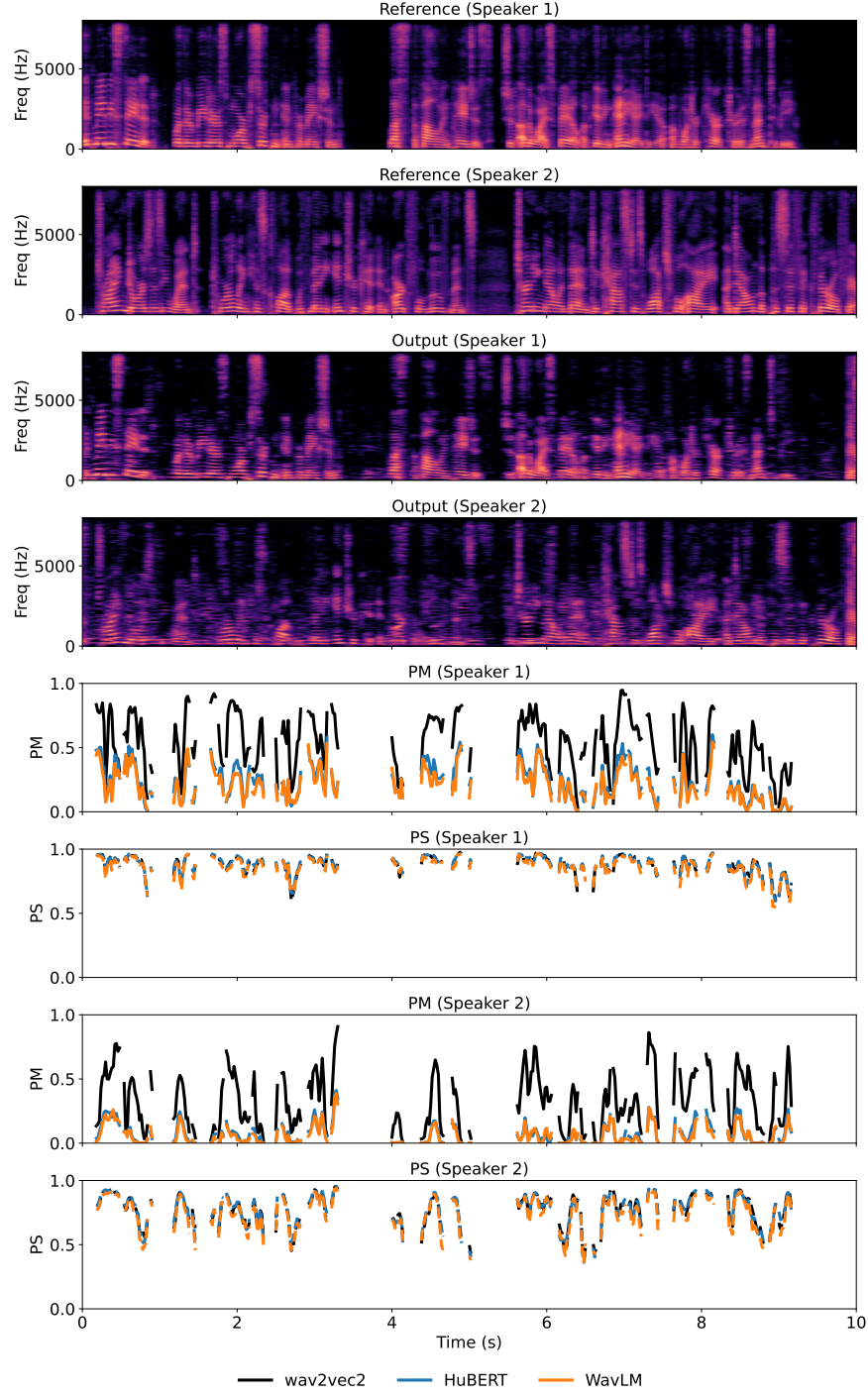


Figure 10: For an English mixture with two speakers, a spectral view of the system signals and aligned with a time-series view of the PS and PM measures of each speaker across different self-supervised architectures. Blank time intervals remain whenever speech does not overlap.

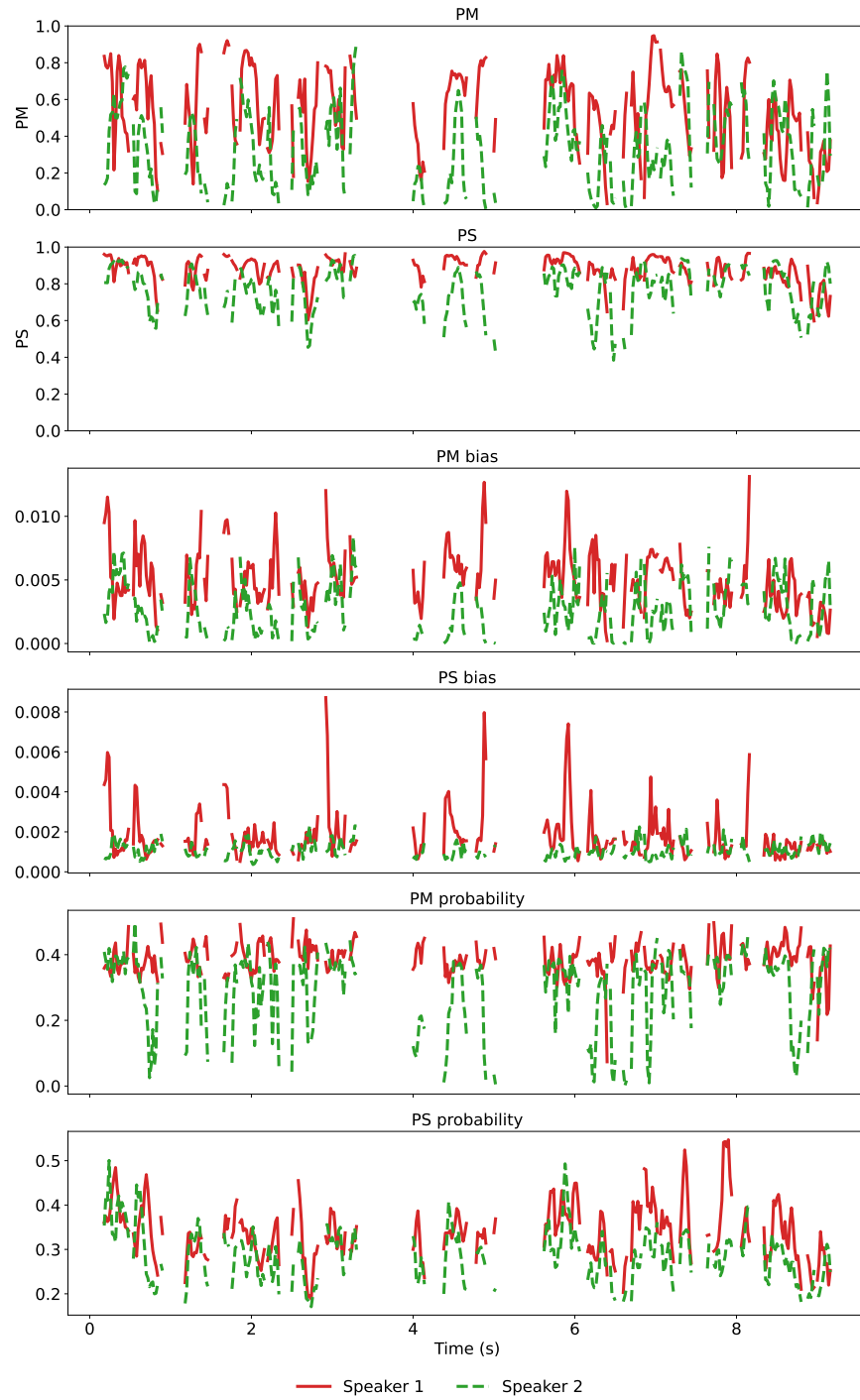


Figure 11: Time-aligned view of the PM and PS measures and their deterministic error radius and probabilistic tail with 95%, of two English speakers. Time indices where speech does not overlap remain blank.

F FRAME COUNTS USED FOR NORMALIZED MUTUAL INFORMATION CALCULATIONS

Threshold	English		Spanish		Music (Drums)		Music (No Drums)	
	PS \leq th	PM \leq th	PS \leq th	PM \leq th	PS \leq th	PM \leq th	PS \leq th	PM \leq th
0.1	583	7426	622	10721	734	14768	1891	46183
0.2	1546	12086	1591	15756	2095	18697	6131	59124
0.3	3191	16350	3350	19714	4392	21496	12748	68927
0.4	5753	20118	6091	23054	8042	23550	22317	76990
0.5	9115	23697	9725	25964	12318	25285	34864	83607
0.6	13364	27232	13904	28627	16135	26892	47411	89667
0.7	18465	30758	18592	30885	19345	28443	59288	95242
0.8	24477	34076	23871	32703	22436	30148	70918	99536
0.9	31572	36507	29589	33902	26080	31397	85541	102589
1	37888	37888	34496	34496	31965	31965	104058	104058

Table 7: Frame counts used for NMI computation at each threshold, denoted ‘th’ in the table. Columns show counts of frames per scenario, split by PS and PM subsets.